

AD-A231 952

DTIC FILE COPY

(4)

Technical Report 1365
December 1990

**A Prototype
Array-Element Localization
Sonobuoy**

J. A. Rice

DTIC
ELECTED
FEB 14 1991
S B D

Approved for public release; distribution is unlimited.

91 2 13 042

NAVAL OCEAN SYSTEMS CENTER

San Diego, California 92152-5000

J. D. FONTANA, CAPT, USN
Commander

R. M. HILLYER
Technical Director

ADMINISTRATIVE INFORMATION

The work described in this report was jointly sponsored by the Office of the Chief of Naval Research, 800 N. Quincy Street, Arlington, VA 22217-5000 and the Naval Air Systems Command, Washington, D.C. 20361-0001. Work was performed by members of several NOSC technical codes.

Released by
M. F. Morrison, Head
Acoustic Branch

Under authority of
J. H. Richter, Head
Ocean and Atmospheric
Sciences Division

ACKNOWLEDGMENTS

The author gratefully acknowledges the contributions of his colleagues and good friends at NOSC, particularly Dr. George Byram, Dr. Newell Booth, Neal Gibsen, Lew Wolfgang, Shelby Sullivan, Mike Morrison, Mike Reuter, Gaylord Doerck, and M. C. Antonio. The expertise of Terry Shepherd and Jim Brown of the Naval Air Development Center, and Joe Grimes, Brian Rehmer, and John Congdon of Magnavox and Paul Hursky of Lockheed was essential to the success of this project.

For their valuable time, interest, and thoughtful suggestions the author is extremely grateful to Dr. Bill Hodgkiss, Dr. Vic Anderson, and Dr. LeRoy Dorman of UCSD.

SUMMARY

OBJECTIVE

Present a design of an array-element localization (AEL) sonobuoy.

RESULTS

1. Development of a prototype AEL (PAEL) sonobuoy.
2. Qualitative validation of PAEL performance by successfully processing experimental sonobuoy arrays.

RECOMMENDATIONS

1. Quantify PAEL accuracy with test arrays in a well-characterized propagation environment using a far-field stationary beacon to project signals of varying source level and frequency.
2. Improve future AEL sonobuoys by
 - a. implementing a reversing frequency modulated sweep direction for successive AEL signals;
 - b. adjusting the AEL signal envelope to take full advantage of the improved transducer response; and
 - c. increasing the detectability of the start pulse.
3. For arrays using directional low-frequency analysis and recording (DIFAR) sonobuoys, ensure compatibility of future AEL sonobuoys with the new type Q-53D DIFAR sonobuoy.



Accession For	
NTIS GRA&I <input checked="" type="checkbox"/>	
DTIC TAB <input type="checkbox"/>	
Unannounced <input type="checkbox"/>	
Justification	
By _____	
Distribution/ _____	
Availability Codes	
Dist	Avail and/or Special
A-1	

CONTENTS

1.0	INTRODUCTION	1
1.1	The Concept of a Sonobuoy Array	1
1.2	Beamforming	2
1.3	The AEL Problem	4
2.0	PROPERTIES OF A SONOBUOY ARRAY	4
2.1	Beamforming Frequency Band	4
2.2	Passive Element Placement Within the Array	4
2.3	Active Element Placement Within the Array	5
3.0	ENVIRONMENTAL OCEANOGRAPHY	7
3.1	Physical Oceanographic Influences	7
3.2	Far-field Acoustic Oceanographic Influences	8
3.3	Near-field Acoustic Oceanographic Influences	11
4.0	CANDIDATE ARRAY ELEMENTS	15
4.1	The LOFAR Sonobuoy	15
4.2	The DIFAR Sonobuoy	16
4.3	Multielement Sonobuoys	19
5.0	REQUIRED AEL ACCURACY	20
5.1	Accuracy of Horizontal Estimation	20
5.2	Accuracy of Vertical Estimation	22
6.0	AEL ALGORITHMS	25
6.1	Data Structures	25
6.2	Refraction and Sound Speed Corrections	26
6.3	Approaches	26
6.4	Depth Estimation	28
6.5	Horizontal Localization	29
7.0	THE AEL SONOBUOY	30
7.1	AEL Sonobuoy Design Constraints	30
7.2	The AEL Ranging Signal	31
7.3	Transmission of the AEL Signal	35
8.0	EXPERIMENTAL VALIDATION	37
8.1	The PAEL Sonobuoy	37
8.2	Test Arrays	38
8.3	Ranging Measurements	38
8.4	Array Element Localization	45
8.5	Beamforming	45
9.0	CONCLUSION	47
10.0	RECOMMENDATIONS	47
11.0	NOMENCLATURE	47

CONTENTS (continued)

12.0 GLOSSARY	50
13.0 REFERENCES	51

FIGURES

1. Sonobuoy array	1
2. Array beam response pattern function	3
3. Beamforming schematic	3
4. Geometric dilution of precision	6
5. GDOP analysis showing CEP contours	7
6. Sound-speed profiles	9
7. Ray trace for far-field	10
8. Ray trace for near-field	11
9. AEL signal reflection from the sea surface	13
10. DIFAR sonobuoys	17
11. DIFAR composite signal spectrum	18
12. Fractional loss as function of AEL errors	21
13. Coupling schematic	23
14. Ranging paths for a subarray	26
15. PAEL signal response	33
16. A chronological sequence of interference regions	35
17. PAEL sonobuoy	39
18. PAEL sonobuoy lower unit	40
19. PAEL signal replica	41
20. Received PAEL signal at $r = 275$ -meter element	43
21. Received PAEL signal at $r = 1710$ -meter element	43
22. Matched-filter response	44
23. Time history of delay measurements	45
24. Plan view of subarray of Array 143	46

CONTENTS (continued)

TABLES

1. Vertical ranging accuracy, dr_z , required to maintain $dr_{xy} = 1$ -meter horizontal ranging accuracy	24
2. Summary of experimental arrays using PAEL sonobuoys	42

1.0 INTRODUCTION

1.1 THE CONCEPT OF A SONOBUOY ARRAY

A sonobuoy is an expendable sonar device, normally deployed from an aircraft. Impact with the sea separates a tethered hydrophone (or string of hydrophones) to a depth determined by the length of the tether. The hydrophone preamplifier conveys an electrical analog of received sound up to the surface float. Here, a VHF radio transmitter frequency modulates and telemeters the audio signal to the aircraft.

Ninety-nine radio frequencies are allocated as available telemetry channels.¹ Conceivably, the monitoring aircraft could simultaneously receive acoustic information from up to 99 independent sonobuoys.

The opportunity exists then, to coherently process the output of an array composed of the hydrophones of many sonobuoys to enhance the detectability, resolution, and bearing of acoustic plane-wave signals. The individual hydrophones, as elements of a large disk-shaped array, allow spatial sampling of an extended field. Together, the array elements form a powerful, highly directional, large aperture sensor. A sonobuoy array is illustrated in figure 1.

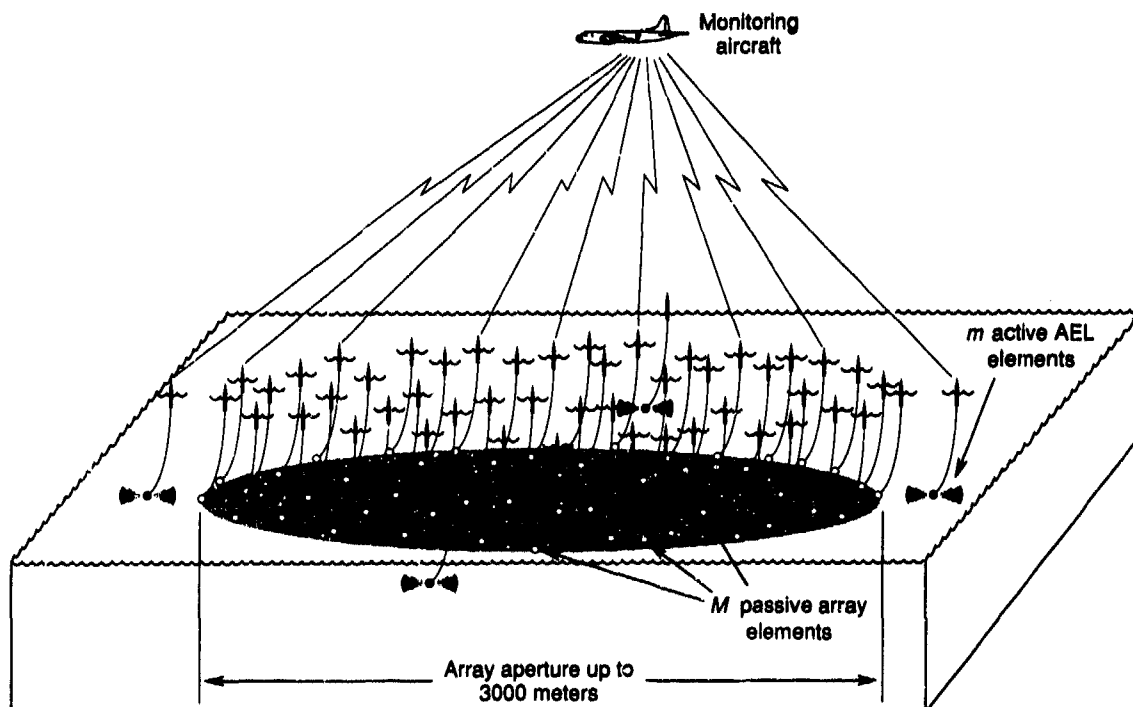


Figure 1. Sonobuoy array.

¹Sonobuoy Instructional Manual, NAVAIR 28-SSQ-500-1, Naval Weapons Support Center, Crane, IN 47522, 1 July 1983.

Array gain is a measure of the increased detectability of signals in the presence of background noise, relative to that of a single hydrophone. For the detection of plane-wave signals, array gain is defined as the signal-to-noise ratio of the directional array to the mean signal-to-noise of a single omnidirectional array element. In decibel units, array gain is

$$G = 10 \log \frac{S/N}{S/N} \quad (1)$$

where S and N are respectively the average signal power and average noise power of the array, and S and N are respectively the average signal power and average noise power of an omnidirectional array element.

Except at extremely low frequencies, the hydrophones of a sonobuoy array can be separated by many acoustic wavelengths, tending to decorrelate element-to-element noise. When the noise field of a sonobuoy array is isotropic, a simplified expression of array gain, the directivity index (DI), may be considered. In this case, array gain is dependent only on the number, M , of array elements. If the array is impinged on by a single, dominant acoustic plane wave in an isotropic noise field, the array signal-to-noise gain approaches

$$G_o = DI_o = 10 \log M. \quad (2)$$

The hydrophone array performs the function of a spatial filter, reducing the ambient noise with which a plane-wave signal must compete and allowing the separate resolution of plane-wave signals arriving from different directions.

1.2 BEAMFORMING

The spatial volume around an array from which incoming acoustic plane waves approach may be divided into discrete angular increments. Signal processing allows the array to be focused on the sound field associated with each solid angle by forming a beam in that direction. The simultaneous formation of many beams yields acoustic response sampled as a function of direction.

Forming a beam in a given direction maximizes the array response to acoustic signals approaching the array from that direction while discriminating against other acoustic energy. The direction in which a beam is formed is defined as the main-response axis and the process of forming a beam is known as beamforming or beam-steering.

Figure 2 depicts a narrowband beam-response pattern function or beam pattern of a simulated random array consisting of $M = 64$ elements uniformly distributed within a 1000-meter horizontal aperture. The main-response axis is steered in the horizontal plane at a bearing of $\theta_{st} = 51$ degrees. The beam pattern includes a mainlobe along the main response axis, as well as sidelobes in directions off the main-response axis. The beam pattern exhibits array gain approaching $G_o = 18$ dB, as predicted by equation (2).

The beamforming process is schematized in figure 3 for a two-dimensional array of $M = 7$ elements. By delaying the output of each array element, the main-response axis is effectively aimed toward some desired look direction. The delay, τ_j , applied to the output of designated hydrophone j is equal to the time required for sound to propagate to the hydrophone from an arbitrary plane perpendicular to the main-response axis. By effectively moving the hydrophones to a plane perpendicular to the main-response axis,

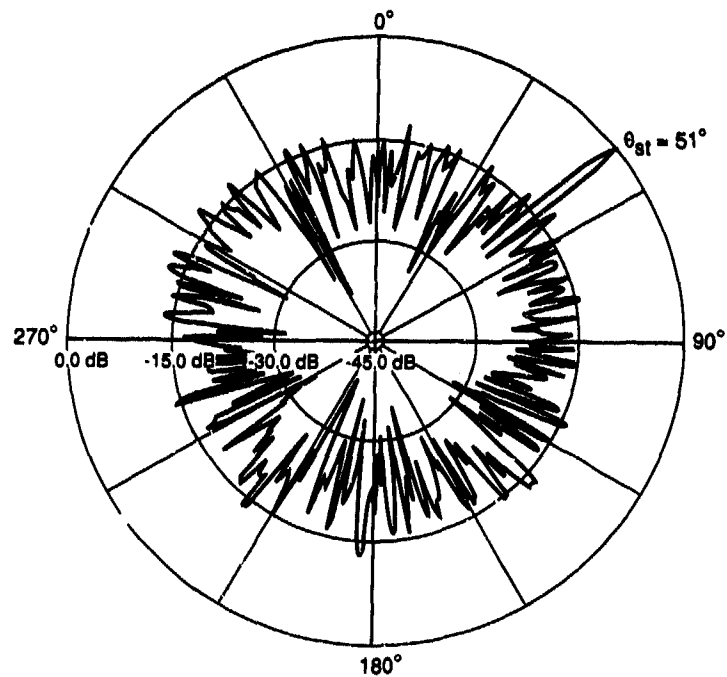


Figure 2. Array beam response pattern function.

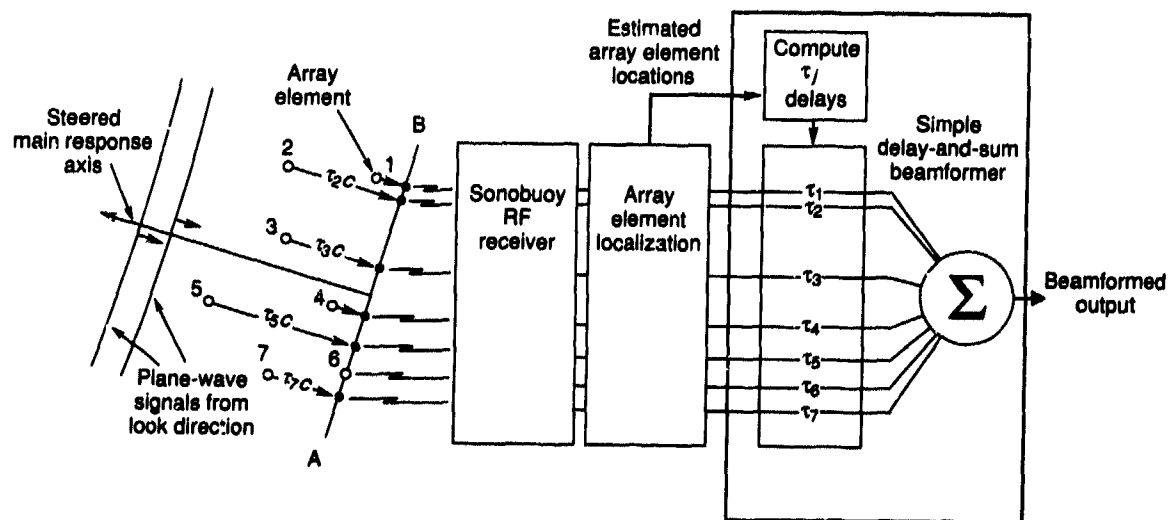


Figure 3. Beamforming schematic.

such as the one described by line AB in the two-dimensional example of figure 3, beamforming results in the alignment of acoustic energy irradiating the array elements from the look direction. When the time-shifted hydrophone outputs are summed, signals approaching only along the main-response axis are reinforced, and array gain is realized.

The key problem in beamforming lies in selecting the appropriate set of time delays, $\{\tau_j\}$. Advanced self-cohering techniques offer the possibility of cohering the array elements by adaptively matching the array output to the noise field itself without knowledge of the element locations. The more conventional approach requires a priori determination of the relative hydrophone locations; these known element coordinates are then used to derive the beamforming delays. The positions of hydrophones in a sonobuoy array must constantly be tracked since the buoys are independent and influenced by the ocean currents. If relative array-element locations are not known to sufficient accuracy, the full potential array gain, G_a , cannot be achieved.

1.3 THE AEL PROBLEM

This report addresses the problem of array-element localization (AEL) in a sonobuoy array.

A solution to the AEL problem is developed by introducing several active acoustic projectors into the array field as illustrated in figure 1. These projectors acoustically survey the passive hydrophones, allowing position estimation of the array elements. Typically four such projectors are deployed per array, each projector suspended from a special AEL sonobuoy. Following transmission of a ranging signal by an AEL sonobuoy, each hydrophone in the array is acoustically illuminated at a propagation time proportional to its distance from the projector. An AEL algorithm is thereby provided with a stream of range measurements from each of the AEL projectors to each array element. In contrast to triangulation procedures using angle measurements to obtain position estimates, the solution described here uses distance measurements and is, therefore, a trilateration process.

2.0 PROPERTIES OF A SONOBUOY ARRAY

2.1 BEAMFORMING FREQUENCY BAND

Since the elements of a sonobuoy array are not physically linked, large array apertures of up to 3000 meters are feasible.

Omnidirectional noise with wavelengths less than $\lambda = 300$ meters is generally uncorrelated when sampled at array elements sparsely distributed over such large apertures. Thus, for signals with $\lambda < 300$ meters, the noise field isotropy assumption is valid and array gain is expressed by equation (2).

Detecting shorter wavelength signals requires a proportional increase in the accuracy to which the array elements are localized. Beamforming of signals having wavelengths of $\lambda > 10$ meters will be demonstrated to be an attainable goal with the AEL system developed in this report.

Consequently, sonobuoy arrays are well-suited for detecting low-frequency acoustic signals, specifically in the 5-Hz ($\lambda_{\max} \approx 300$ meters) to 150-Hz ($\lambda_{\min} \approx 10$ meters) range.

2.2 PASSIVE ELEMENT PLACEMENT WITHIN THE ARRAY

Stock sonobuoys typically allow hydrophone elements to operate 30, 120, or 300 meters beneath the ocean surface. These standard depth settings are commonly called shallow, intermediate, and deep, respectively. Elements of a sonobuoy array are normally deployed at the same operating depth, creating a

horizontal array aperture with minimal thickness. Use of mixed operating depths would result in premature dispersion of the array by shear currents acting on the dissimilarly configured buoys. The average horizontal element spacing, in a probabilistic nearest-neighbor sense, of a disk-shaped array containing M randomly located and uniformly distributed elements is

$$\begin{aligned} F &= r_{\max} 4(M-1) \left[\frac{(M-1)/(M-1)!}{(2M-1)!} \right] \\ &\approx r_{\max} \frac{0.88}{\sqrt{M}}, \end{aligned} \quad (3)$$

where r_{\max} is the array diameter.

The directivity index increases with M , but saturates when F reaches one-half the signal wavelength.

Quite often, the horizontal distribution of hydrophone elements in a sonobuoy array is thinned, signifying that the mean interelement spacing is greater than one-half the largest wavelength associated with the beamforming frequency band,

$$\begin{aligned} r &> \frac{\lambda_{\max}}{2} \\ &> 150 \text{ meters}. \end{aligned} \quad (4)$$

Although a thinned array is spatially undersampled, the mainlobe beamwidth is not degraded since its properties are determined by the aperture of the array. However, since the number of elements in a thinned array is reduced, the average sidelobe level is higher than would be expected from a fully sampled array of the same aperture. Let the mainlobe amplitude be M , as would be expected for an array of M normalized and perfectly localized elements each contributing a cophased vector in the direction of the main-response axis. In a given direction away from the main-response axis, though, the vectors are not cophased due to the random element locations and instead exhibit statistically random phases. The unit vectors combine with random phase to produce a sidelobe level with root mean square (rms) amplitude of \sqrt{M} . For a random array, therefore, the power ratio of the average sidelobe to the mainlobe is $M/M^2 = 1/M$ (Lo, 1964, 1965).

A more insidious threat to performance of a thinned array is the possibility of grating lobes. If spatial periodicity exists in the element positions, coherent buildup of cophased unit vectors in directions away from the main-response axis results. Grating lobes in the radiation pattern arise from the convolution of the beam pattern of the nonsampled aperture with the Fourier transform of the spatial sample distribution. Grating lobes will therefore fail to arise if periodicity in the element locations is avoided (Steinberg, 1976).

Because of the inherent irregularity and unpredictability of element placement when launching sonobuoys from an aircraft, and because of the effects of wind and ocean currents, randomization of the array field occurs naturally as long as the deployment provides fairly uniform coverage of the array field.

2.3 ACTIVE ELEMENT PLACEMENT WITHIN THE ARRAY

Careful placement of the AEL sonobuoys around the perimeter of the array is extremely important if accurate element localization is to be achieved. This is due to a phenomenon called geometric dilution of precision (GDOP) (Cheung and Warren, 1978). Acoustic surveying of an array element from a projector will result in a range measurement that contains some measurement errors from uncorrected acoustic

refraction, quantization, or round-off errors. When combinations of such measurements are used to trilaterate the location of a hydrophone, the result is inaccurate position estimation.

The fundamental principle underlying GDOP is illustrated in figure 4, which shows two AEL sonobuoy reference points and an estimated array element location in the array field. The intersection of the two annuli represents the region in which the trilaterated element is located, given rms range-measurement errors, σ_r , corresponding to the annuli widths. A region of intersection is often represented as an ellipse and is referred to as an error ellipse. In figure 4(a), the GDOP effect is large since the two AEL references are nearly colinear with the trilaterated array element. On the other hand, in figure 4(b), the two AEL reference points have nearly optimal angular separation resulting in minimal GDOP.

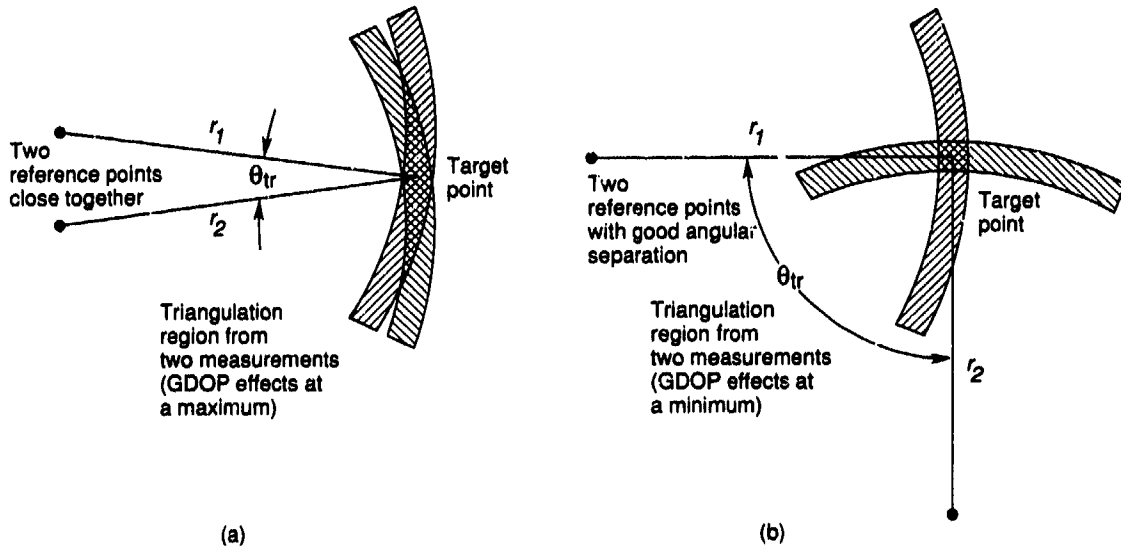


Figure 4. Geometric dilution of precision.

From the above example, it is observed that the uncertainty of the estimated location in the direction perpendicular to the axis of measurement may be much greater than the measurement error. Moreover, when two reference points are close together, the uncertainty of the estimated location is greatest in the direction perpendicular to the bisector of the trilateration angle, θ_{tr} . While the minor axis of the error ellipse is approximately equal to the range-measurement error, σ_r , the major axis is relatively large. But when two reference points are situated such that the lines of measurement are perpendicular to one another, the area of overlap is minimum. The major and minor axes of the error ellipse are both approximately equal to the range-measurement error.

AEL-sonobuoy placement at the corners of a square is ideal (Cheung et al., 1978). In the region contained by the square, excluding those areas in the vicinity of the AEL sonobuoys, array elements are optimally localized.

GDOP analysis of any AEL-sonobuoy placement geometry may be performed using techniques first developed for radar applications. Given some margin of error in the locations of the AEL projectors, the circular equal probability (CEP) is computed for points throughout the array field. The CEP for a given point is a measure of how accurately an array element located at that point can be localized using the imperfectly localized AEL projectors and inexact range measurements from each of the AEL projectors to that point. By convention, the CEP is the value of the radius of a circle in which there is a 50-percent probability that the array element is located therein. A complete GDOP analysis of an AEL-placement

geometry would result in a contour plot showing lines of constant CEP for the two-dimensional array field. GDOP analyses are presented for the ideal AEL-sonobuoy placement case in figure 5(a) and for a poor AEL-sonobuoy placement case in figure 5(b).

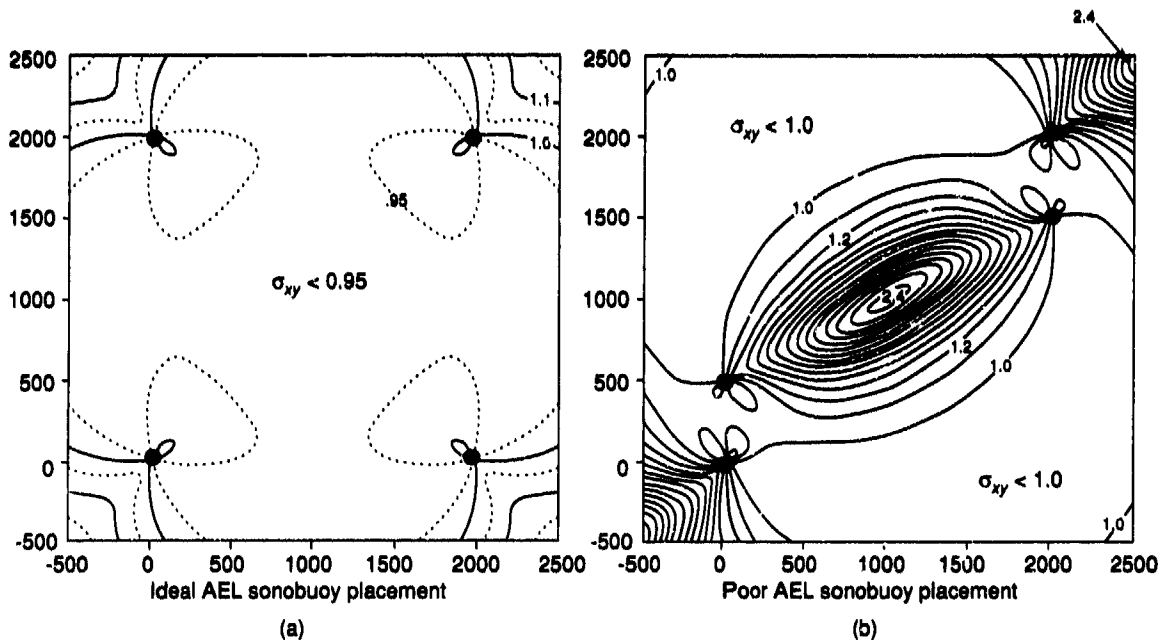


Figure 5. GDOP analysis showing CEP contours.

Both GDOP analyses assume that the rms positional uncertainty of the AEL reference points is $(\sigma_{xy})_{AEL} = 0.5$ meter and that the range measurements suffer from an rms error of $\sigma_r = 1$ meter. Note the extremely poor localization performance in the center region of the array field of figure 5(b).

The ideal placement strategy must form the basis for any successful sonobuoy array deployment. To execute the strategy requires careful consideration of the pragmatics of deployment from an aircraft, usually a Navy P-3, flying at 200 knots with no visual references over an array area it traverses in less than 30 seconds. P-3 facilities for marking on top of already deployed buoys and geo-correcting the computerized navigation system based on these inputs must be relied upon. Deployment schemes making use of these tactical tools may not directly lend themselves to the deployment of optimal array geometries.

A potential approach is to deploy the array all at once from the bomb bay of the aircraft. The buoys would disperse automatically from a single magazine pod and glide to a predestined impact point on the ocean surface. Special aerodynamics of the individual buoy canisters would assure uniform element dispersion and equispaced placement of the four AEL buoys about the array perimeter. While this suggestion has many merits, the engineering hurdles in implementing it with existing aircraft and existing sonobuoy designs are large indeed.

3.0 ENVIRONMENTAL OCEANOGRAPHY

3.1 PHYSICAL OCEANOGRAPHIC INFLUENCES

Because sonobuoys occupy the water column from the sea surface to as deep as 300 meters, they are acted on by surface winds and subsurface flow. Ocean currents vary greatly in direction and intensity as a

function of location and depth. However, the array aperture covers a small area with respect to major atmospheric and oceanic circulation processes. If the buoys are all deployed to the same operating depth and are hydrodynamically similar, the net drag forces acting on them are approximately the same and the array field is transported en masse. This group buoy migration has an insignificant impact on the functioning of the array since Doppler distortion from absolute sonobuoy drift is small over beamforming integration times. Far-field targets can be tracked relative to the slowly moving array since the array position is tracked accurately by the monitoring aircraft.

A more significant effect of ocean currents is relative motion of the individual array elements. Relative sonobuoy drift is the result of slight differences in buoy-to-buoy drag characteristics, nonuniform surface wind stresses, and the fact that ocean currents are turbulent. Turbulent flow is characterized by an irregular and fluctuating velocity field.

During a sea test in which candidate AEL ranging signals were being projected from a large transducer, propagation measurements to receiving sonobuoys at various ranges were desired. The transducer was suspended 300 meters below a barge moored in deep water in the Caribbean Sea. While the original experiment plan called for a workboat to ferry the buoys out to the desired ranges, it was found that the absolute sonobuoy drift was substantial enough that the buoys could simply be thrown from the barge and the currents would carry them away from the stationary barge. Since pairs of like buoys thrown simultaneously from the barge maintained similarly increasing ranges from the projector, it was noted that relative sonobuoy drift was quite small with respect to the absolute sonobuoy drift. However, a pair of type Q-53B buoys manufactured by two different companies experienced higher relative sonobuoy drift rates than another pair produced by the same manufacturer. This observation counsels that arrays be populated with buoys from the same manufacturer to assure similar drag characteristics. The further precaution of populating arrays with buoys from the same production lot eliminates effects of design evolution and reduces effects of production variability on relative drift-rate performance.

Relative-drift rates as high as 2 meters/minute for the type Q-57 sonobuoys have been observed. Type Q-53B relative-drift rates measured in experimental arrays have ranged from 0.0 m/min to 0.5 m/min. Severe dispersion is thwarted by selecting the deep operating depth where the sonobuoy drogue tends to anchor the array elements in the uniform ocean currents beneath the mixed layer.

Consideration of relative-drift rates will be important in the mechanical design of the AEL sonobuoy and in the required update rate of array element positions.

Inference of the array orientation by observing the sonobuoy surface floats is inexact since the relative locations of the hydrophones do not necessarily correspond to the relative locations of the surface floats. Moreover, techniques at the disposal of the monitoring aircraft by which relative locations of surface floats are determined are very crude when compared to available acoustic orientation techniques.

3.2 FAR-FIELD ACOUSTIC OCEANOGRAPHIC INFLUENCES

Sound speed is a function of the density and bulk modulus of elasticity of the medium. In the ocean, these parameters vary both temporally and spatially since density depends on the chemical composition of the water, and the bulk modulus depends on both temperature and pressure. Empirical and theoretical expressions for sound speed in terms of temperature, salinity, and depth are available (Urick, 1983; Burdick, 1984; and Mackenzie, 1981).

A sound-speed profile (SSP) shows sound speed as a function of depth in the water column for a given environment. SSPs characteristic of specific oceanic regions during particular seasons have been extensively compiled. Typical SSPs for selected areas are plotted in figure 6. The SSP may be derived in the field by combining measured or historical salinity for the area with a measured temperature profile,

typically obtained using bathythermography. From the aircraft, a type Q-36 bathythermograph is used to obtain a temperature profile.

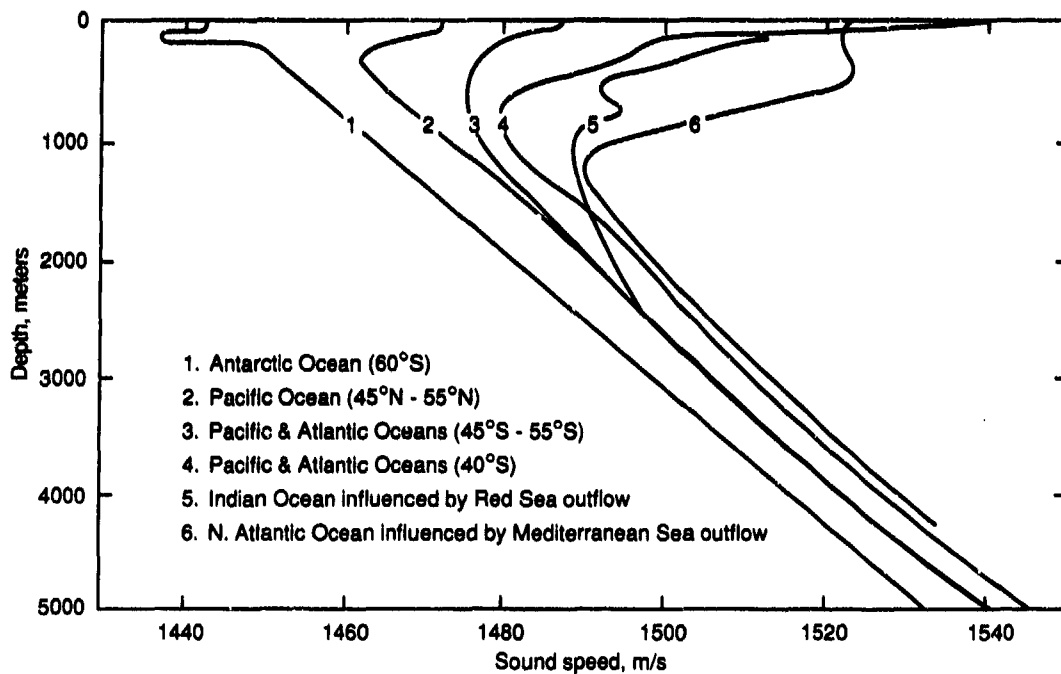


Figure 6. Sound-speed profiles. (Urick, 1983).

Snell's Law governs refraction of sound waves induced by sound-speed gradients. Ray theory provides convenient methods of tracing propagation paths and is useful for analyzing sound distribution and the effects of boundary conditions.

Ray-trace diagrams for sound originating at various depths are presented as figure 7. The horizontal range scale is greatly compressed to show propagation structure over great distances.

As demonstrated by figure 7, sound emitted by an acoustic source is refracted away from regions of high sound speed such that a deep sound channel is created. Near the surface, ray paths intersect and sound is focused into periodic convergence zones where relatively high sound intensities occur.

Since stock sonobuoys operate at nominal depths of 120 meters or 300 meters, it is interesting to examine the relative properties of distantly propagated sound at these two receiver depths. If the receiver is at a convergence zone, ray theory suggests that the greatest sound intensities from the source are found at the source depth, where propagation paths focus. For a given source, however, convergence zones of emanations from that source cover only narrow annular areas of the ocean. This focusing actually acts to the disadvantage of a detection system at the source depth since it is very unlikely that the receiver will find itself in the convergence zone. Even if the fairly large aperture of the sonobuoy array intersects the narrow annulus, only a subset of the array elements may be stimulated. The most favorable deployment strategy, as is supported by near-field propagation considerations, is to place the array at the deep operating depth. Although convergence-zone propagation is less focused here, the wider annulus of convergence increases the probability of detection of signals from near-surface sources and allows for more uniform exposure of the entire array aperture. Uniform exposure equalizes the SNR across the array, allowing fuller realization of array gain.

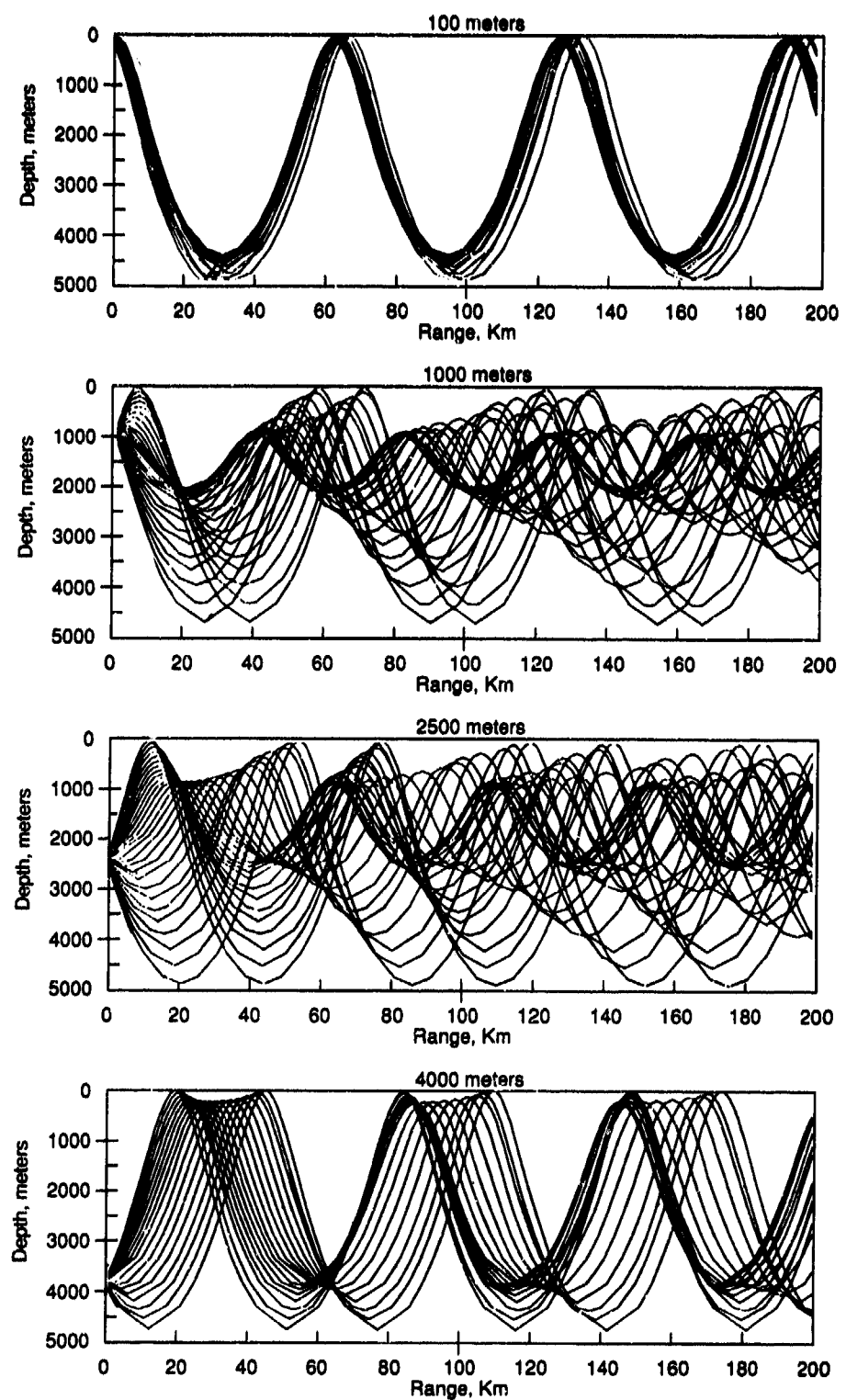


Figure 7. Ray trace for far-field. (Urick, 1983).

For arrays at the deep operating depth having apertures approaching 3000 meters, the planar wavefront assumption is not necessarily valid. Since uncompensated wavefront anomalies have the same effect as AEL errors, signal coherence must be considered in the design of the beamformer. The presence of multiple arrival angles and local sound-speed variations within the extent of the array can degrade the performance of simple delay-and-sum beamforming, suggesting that a more sophisticated beamformer may be required.

The arrival angle of deep sound-channel propagation at the deep and intermediate sonobuoy operating depths is $\psi_{st} < \pm 18$ degrees, where ψ_{st} is measured from the horizontal. The vertical arrival structure of sound is a phenomenon which could be exploited by judicious design of the vertical directional response of the passive elements. Discrimination by the array elements against directional noise is useful only to the extent that the localization-ranging signals are not excluded.

An effective method of geographically orienting the array requires a distant acoustic source with known transmission characteristics and known location. Orientation of the array using this approach must be performed subsequent to beamforming since the formed beams are used to detect the far-field beacon source.

3.3 NEAR-FIELD ACOUSTIC OCEANOGRAPHIC INFLUENCES

Far-field ocean acoustics have been considered for the detection and tracking of distant sound sources. Before the AEL problem is treated, for which the array elements may be viewed as analogous to local targets to be detected and tracked, near-field acoustics must be examined.

The AEL sonobuoys project acoustic ranging signals, hereafter referred to simply as AEL signals, which are sensed by the array elements. Since GDOP analysis supports the placement of the AEL buoys at or outside the array perimeter, the distance from an AEL projector to a given receiving hydrophone could be as great as the maximum array aperture of 3000 meters.

For a typical North Pacific SSP, plotted in figure 8(a), near-field ray-trace analyses for AEL signals projected from the intermediate operating depth of 120 meters and from the deep operating depth of 300 meters are presented as figures 8(b) and 8(c), respectively. The SSP is generally assumed to be applicable for the entire horizontal aperture of the array. To reduce relative drift, the array elements are generally located at the same operating depth as the AEL projector. The dashed line in each diagram, therefore, represents both the AEL-projector-source depth and the receiver depth of the entire array.

The curved paths along which the sound rays travel expose the AEL signal to nontrivial, depth-dependent variations in sound speed.

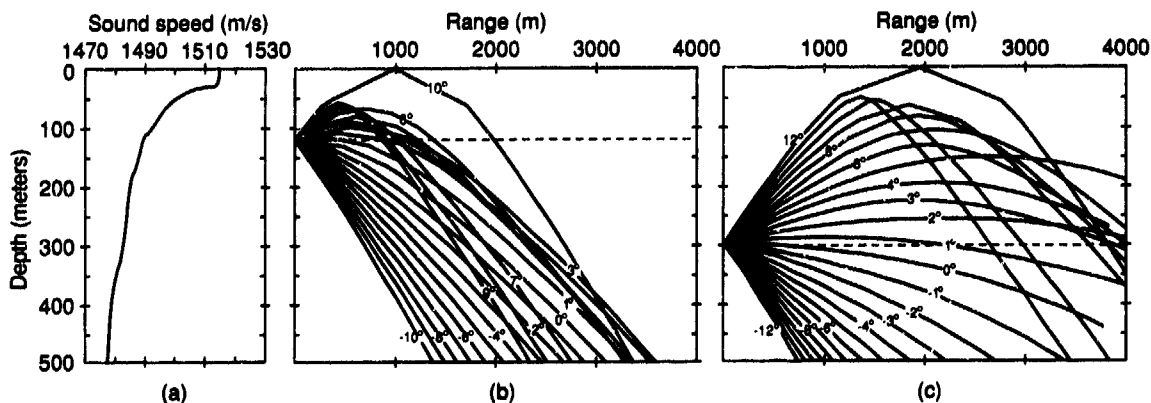


Figure 8. Ray trace for near-field.

Observe in figure 8(b) that array elements more than 2000 meters from the AEL projector lie in a shadow zone. Shadow zones are regions acoustically illuminated only by way of bottom reflection, sea surface scattering, or dispersive processes. Array elements in a shadow zone of an AEL projector, therefore, cannot be acoustically surveyed by that projector. Figure 8(b) exposes a major restriction of sonobuoy arrays deployed at the intermediate operating depth. To be localized, the array must not have an aperture extending into the shadow zone of its AEL sonobuoys. The array aperture could expand during the life of the array due to relative sonobuoy drift, introducing shadows at the array fringes.

On the other hand, the proximity of the shadow zone in figure 8(c) is more distant than the desired 3000-meter array aperture. The deep operating depth is therefore favored by both far-field and near-field acoustic propagation considerations.

Prior to deploying an array in a particular environment, near-field ray-trace analysis is recommended for the desired operating depth of the sonobuoys. Shadow zones for the expected SSP may then be identified in advance and array apertures may be knowledgeably selected. Figure 8 also provides a graphic demonstration of multipath propagation of the AEL signal. Typically, a direct path and a surface-reflected path may be identified for most ranges within the array aperture.

The surface-reflected ray projected vertically upward is of special interest since the echo returns to the AEL element. This fact may be exploited to measure the depth of the AEL projector. A vertical ray is especially useful since refraction is insignificant for paths perpendicular to the typically horizontal isopycnals.

In some environments the SSP may be closely approximated by a constant negative gradient,

$$\frac{\partial c}{\partial z} = \text{constant} < 0, \quad (5)$$

under the influence of which all sound rays are refracted downward. With this approximation, the angle of departure, ψ_{gr} , of the ray which just grazes the sea surface before being refracted downward may be estimated as

$$\psi_{gr} = \cos^{-1} \left[1 + \frac{z \frac{\partial c}{\partial z}}{c_o} \right], \quad (6)$$

where c_o is the sound speed at the sea surface and z is the AEL sonobuoy operating depth. All rays that leave the projector at angles greater than ψ_{gr} will be surface-reflected toward deep water. Under the uniform-gradient assumption, no rays can extend beyond the surface-grazing ray. The grazing ray, therefore, represents the boundary of the shadow zone. Making use of the fact that, in a constant gradient medium, rays describe the arc of a circle, the maximum useful array aperture may be estimated using the formula for horizontal chord length,

$$r_{xy} < - \left[\frac{2c_o}{\frac{\partial c}{\partial z}} \right] \sin \psi_{gr}. \quad (7)$$

Following projection of an AEL signal, the hydrophone element of each sonobuoy is encountered first by the direct-path acoustic transmission. The surface-reflected-path echo of the AEL signal reaches the

element shortly thereafter. Simulation has confirmed the precedence of the direct path for ranges of 3000 meters and less. In even the most extreme open-ocean acoustic environment known, that of the southern Japan Sea where extreme sound-speed gradients between the surface and 300-meter depth occur, the direct path is not preceded by the surface-reflection until ranges of 3100 meters and beyond.

For a typical SSP such as that shown in figure 8(a), the time difference between the direct-path and surface-reflected-path arrivals at the deep operating depth varies from 400 ms to 25 ms as range, r_{xy} , increases from 0 to 3000 meters.

The ray curvature of the transmission paths in figure 8 indicates that refraction is significant. AEL signals are refracted as they propagate across the array aperture and the difficulty of fully compensating for this effect is a primary source of AEL error. Comparing rays of locally produced signals with those of distantly produced signals reveals different behavior within the locale of the array. AEL errors due to refraction of the ranging signal normally do not cancel the beamforming errors caused by far-field refraction. It is not sufficient therefore, to neglect the effects of refraction when localizing the array elements. Array-element positions should be determined in an unwarped reference system by attempting to convert the AEL-signal-travel-time measurements to unrefracted distances.

The surface-reflected-path measurement is particularly sensitive to refraction and sound-speed variations since it is affected by near-surface sound-speed gradients. Algorithms are required to derive the direct and surface-reflected, straight-line range from the measured, direct and surface-reflected propagation-path arrivals. Using the local SSP and the estimated AEL projector source depth, these algorithms would, in essence, perform the inverse function of a ray-trace algorithm (Officer, 1958; Eby, 1967; and Hunt, Marquet, Moller, Peal, Smith, and Spindel, 1974).

Consider now the physics of a surface-reflected signal. Surface-reflected sound waves are phase-shifted by 180 degrees upon reflection at the water-air interface. These result in sound pressure having a sign opposite to that produced by nonreflected sound waves.

Figure 9(a) depicts the reflected path from a sea surface that is smooth and is, therefore, a perfect reflector. For simplicity, the sound-speed gradient is assumed to be zero, resulting in nonrefracted paths. At the receiving hydrophone, the reflected signal appears to have originated at a point above the sea surface that corresponds to the image of the AEL projector location, with equal amplitude but opposite sign compared with the nonreflected, direct-path signal.

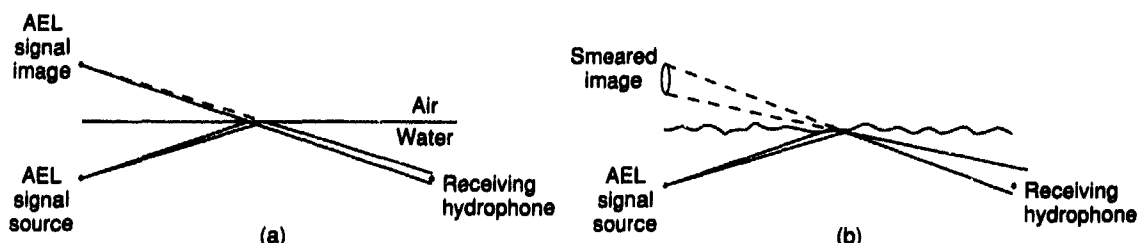


Figure 9. AEL signal reflection from the sea surface.

If the AEL signal is a tone, there is danger of constructive and destructive interference at a receiver by the direct and surface-reflected signals. This image interference can inhibit localization efforts.

Since the sea surface is not perfectly smooth, the rays are reflected in ever-changing directions according to the faceting of the reflective interface. Figure 9(b) is representative of a rough surface condition. Viewed from the receiving element, the image of the AEL projector is smeared such that the apparent image intensity is reduced. Reflection loss occurs as the result of this diffusive phenomenon. Reflection loss of a 2-kHz signal ranges from 0 dB in sea state 1 to 10 dB in sea state 6 (Burdick, 1984).

The Rayleigh criterion provides a guideline for determining whether a reflective surface is smooth relative to the wavelength of the signal being reflected. Rayleigh's smoothness criterion states that the surface may be considered smooth if the path difference between rays reflected from the top and bottom of the surface irregularities is less than $\frac{1}{4}$ wavelength. The reflection loss may be assumed, therefore, to be zero for signal frequencies smaller than

$$f < \frac{c}{16 \pi H \sin \theta_{gr}} , \quad (8)$$

where H is the rms wave height measured from crest to trough, and θ_{gr} is the grazing angle at which the sound ray would strike a horizontal sea surface. By this criterion, we find that even in sea state 1 with $H = 0.2$ meter and for a grazing angle $\theta_{gr} = 90$ degrees, that for frequencies above $f = 150$ Hz the sea surface must be considered rough (Rice, 1990).

If the AEL signal is designed to give sufficient processing resolution, the model of incoherent summing of signals from a large surface area does not apply. Instead, the surface roughness is overresolved and multiple, specularly reflected surface-path arrivals can be expected at the receiving hydrophone. The first surface-reflected-path arrivals best represent the idealized surface-reflected path.

Reflection loss and surface scattering loss are offset by a focusing effect refraction has on the surface-reflected path. This effect is readily seen at the operating depths of figure 8 where the density of surface-reflected rays is greater than that of rays which have taken the direct route. This concentration of acoustic energy results in higher intensities for the surface-reflected path than would be expected under spherical spreading assumptions. Use of ray density to infer relative signal intensity is valid here since the rays have equal angular spacing at the source.

As the AEL signal propagates across the array aperture, it will suffer a loss in signal level called acoustic transmission loss. For a range of $r = 3000$ meters and an absorption coefficient at 2000 Hz of $\alpha = 0.13$ dB/km (Thorp, 1965), the transmission loss (TL) can be expected to be approximately (Urick, 1983)

$$\begin{aligned} TL &\approx 20 \log r + \alpha r \times 10^{-3} \\ &\approx 69.54 \text{ dB} + 0.39 \text{ dB} \\ &\approx 70 \text{ dB} , \end{aligned} \quad (9)$$

where the first term accounts for spherical spreading of the projected signal and the second term, insignificant in this case, is volume attenuation. Acoustic propagation modeling using the RAYMODE program for the SSP of figure 8 was performed. RAYMODE is particularly useful in quantifying the effects of temperature gradients on simulated signals. For a 300-meter source depth, TL was predicted to be as high as

$$TL \approx 78 \text{ dB} .$$

(10)

Because it takes into account the actual environmental influences on sound propagation, this prediction is considered to be more realistic than the spherical spreading assumption estimate.

The AEL signal must perform amid a background of ambient noise. The dominant source of ambient noise in the 500-Hz to 20-kHz spectrum is wind-induced surface disturbance (Wenz, 1964 and Ross, 1987) including processes such as breaking whitecaps, spray, bubble formation and collapse, and turbulent pressures in the air coupling directly into the water. Since acoustic energy in this frequency regime is rapidly absorbed and because of the geometric properties of the sea surface as a radiator, wind-related ambient noise is more intense in the vertical direction than in the horizontal direction (Burdick, 1984). The sea state in the locale of the sonobuoy array is, therefore, a direct indication of the ambient-noise level with which the AEL system must compete. The Knudsen curves (Knudsen, Alford, and Emling, 1944) which empirically relate noise spectrum level to sea state, indicate that ambient-noise levels from 45 to 65 dB re $1 \mu\text{Pa}/\sqrt{\text{Hz}}$ may be expected from sea state 1 to sea state 6, respectively. For a sonobuoy array in sea state 6, the ambient-noise level to be used when designing the AEL signal is

$$NL = 65 \text{ dB re } 1 \mu\text{Pa}/\sqrt{\text{Hz}} .$$

(11)

The issue of signal-to-noise, as a design parameter of the AEL signal, is deferred for later discussion.

4.0 CANDIDATE ARRAY ELEMENTS

4.1 THE LOFAR SONOBUOY

The AN/SSQ-57A sonobuoy,* often abbreviated Q-57A and referred to as the Low-Frequency Analysis and Recording (LOFAR) sonobuoy, is a fairly simple buoy. It has a single omnidirectional hydrophone with a frequency response ranging from 10 Hz to 20 kHz. Now in production is the Q-57B sonobuoy, similar to the Q-57A in all respects except for the suspension system and frequency response.

For use in sonobuoy arrays, these buoys have two very serious disadvantages.

The first disadvantage is the limited operating depth. The maximum depth to which the Q-57A and Q-57B hydrophones may be deployed is the intermediate operating depth of 120 meters. In most environments, the useful aperture of an array of Q-57s is thereby limited due to the fact that AEL signals do not project into shadow zones caused by acoustic refraction induced by negative sound-speed gradients. The depth limitation also prevents deployment of the array in deeper water where long-range sound propagation from distant targets is generally more favorable.

The second disadvantage is the fact that these buoys are only manufactured for 31 of the 99 available sonobuoy radio frequencies, limiting the number of elements in the array. Furthermore, the buoys are preset at the factory to one of the 31 channels, resulting in inventory difficulty and preflight array-preparation inflexibility.

*See footnote #1 on page 1.

The Q-41B buoy is an earlier version of the LOFAR sonobuoy. The Q-41B has the desirable option of deployment to the deep depth. The Q-41B buoys are presently being produced only for foreign navies, however. Like the type Q-57 sonobuoy, the Q-41B is limited to the 31-channel subset of available radio frequencies.

Several experimental LOFAR sonobuoys have been produced which, in at least one respect, are well suited for use in sonobuoy arrays. These are the VLF sonobuoys, variations of the Q-57A which have reduced mechanical and electrical self-noise. These sonobuoys are responsive below 10 Hz and, therefore, complement the directional VLF capability of a wide aperture, thinned sonobuoy array.

4.2 THE DIFAR SONOBUOY

The U.S. Navy presently uses the AN/SSQ-53B sonobuoy² for the majority of its air-antisubmarine-warfare surveillance operations. The buoy identifier is often abbreviated Q-53B and the buoy is commonly referred to as the DIFAR (directional LOFAR) sonobuoy. A stock Q-53B is shown in figure 10(a). It is produced in large quantities by several competing manufacturers. The large quantity production of this buoy makes it inexpensive and readily available.

Besides an omnidirectional hydrophone, the DIFAR buoy has two orthogonal gradient phones with cardioidal response patterns. The information received by these directional hydrophones is combined with magnetic compass information to determine the azimuthal bearing of sound sources.

The sonic receive system is defined as being all the elements that pass acoustic energy from the ocean through the sonobuoy VHF transmitter. The frequency response of the Q-53B sonic receive system covers the 10-Hz to 2400-Hz range. The Military Specification of the Q-53B prescribes the relationship between the rms sound pressure level of the sound field and the resulting VHF carrier deviation. Allowable tolerance limits of this acoustic sensitivity relationship are given as a function of frequency. Any unwanted signals attributable to the sonobuoy which pass through any part of the sonic receive system and produce a frequency deviation of the VHF transmitted carrier are due to either electrically induced noise or mechanically induced noise. Required noise limitations as a function of frequency are provided by the Military Specification of the Q-53B.

The composite signal used to frequency-modulate the VHF carrier contains the frequency multiplexed output of the three hydrophones. Figure 11 shows the spectrum of a typical Q-53B composite signal.

The composite signal is the sum of the following five component signals:^{*}

- a. **Omni channel.** The audio output of an omnidirectional acoustic receiver.
- b. **Phase pilot.** A constant amplitude 15.0 kHz (± 50 Hz) phase reference signal from which the subcarrier of the cosine channel and the sine channel is derived. The frequency and amplitude of the phase reference signal are specified such that they may not vary more than 1 Hz/s or 1 dB/s, respectively.
- c. **Frequency pilot.** A constant amplitude 7.5 kHz (± 25 Hz) frequency reference signal exactly one-half the frequency of the phase pilot. The frequency pilot is located in a quiet frequency region of the composite signal and is provided to more robustly lock onto the phase pilot.
- d. **Cosine channel.** The frequency-multiplexed audio output of a dipole gradient hydrophone acoustically oriented for maximum sensitivity to signals along the reference axis of the sonobuoy. The cosine

²Military Specification, Sonobuoy AN/SSQ-53B, draft MIL-S-81487D(AS), Naval Air Systems Command, Washington, D.C. 20361-0001, 15 May 1983.

^{*}See footnote #2.

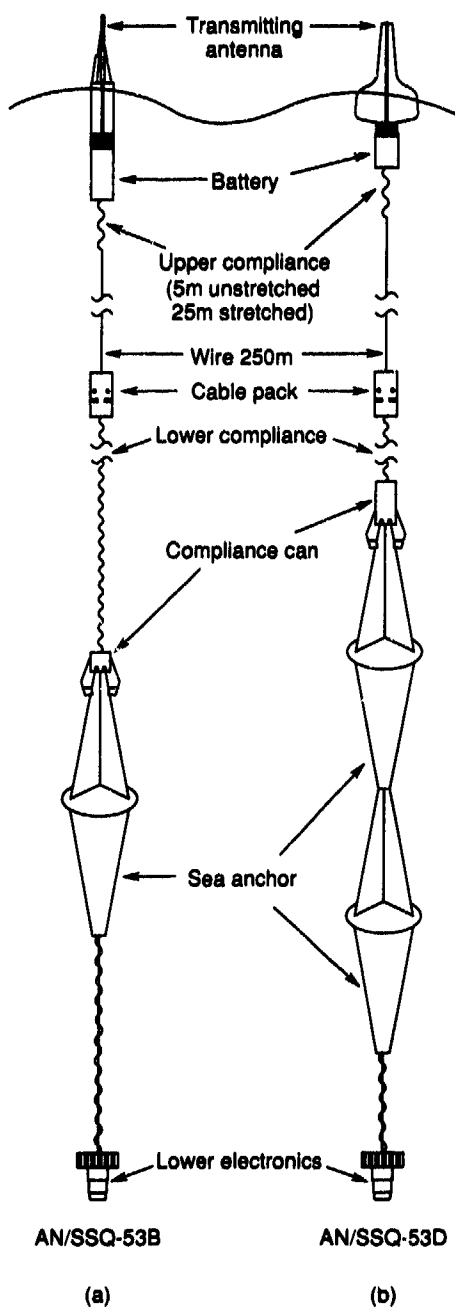


Figure 10. DIFAR sonobuoys.

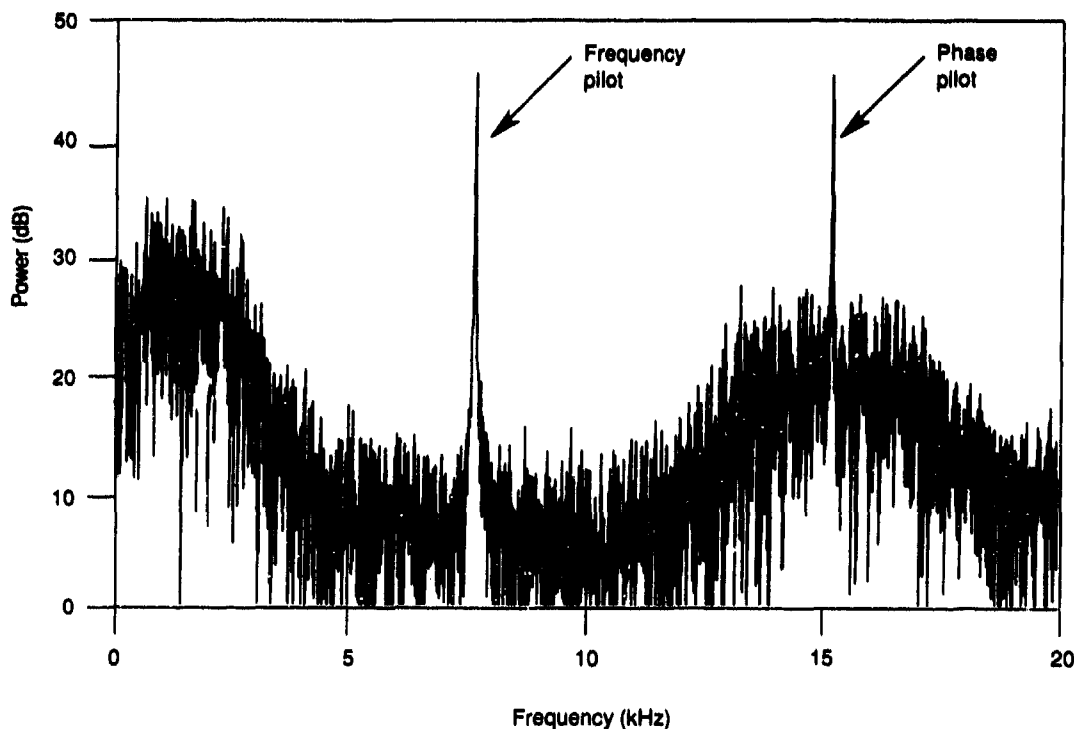


Figure 11. DIFAR composite signal spectrum.

signal is in phase with respect to the omnidirectional signal for acoustic excitation originating within ± 90 degrees of the positive reference axis and is phased 180 degrees with respect to the omnidirectional signal for acoustic excitation originating at angles greater than ± 90 degrees of the positive reference axis. The cosine channel modulates a 15-kHz subcarrier phased to lead the reference phase of the phase pilot by the sum of 90 degrees plus the clockwise angle (as viewed from above) from magnetic north to the positive reference axis of the sonobuoy. The subcarrier frequency is exactly equal to that of the phase pilot.

e. Sine channel. The frequency-multiplexed audio output of a dipole gradient hydrophone acoustically oriented for maximum sensitivity to signals along an axis at right angles to the reference axis of the sonobuoy. The sine channel is in phase with respect to the omnidirectional signal for acoustic excitation originating in the first two quadrants clockwise (as viewed from above) of the positive reference axis. The sine channel modulates a 15-kHz subcarrier phased to lead the subcarrier of the cosine channel by 90 degrees. The subcarrier frequency is exactly equal to that of the phase pilot.

The operating depth of the Q-53B hydrophone and suspension system is selectable prior to launch. Shallow depth, intermediate depth, or deep depth may be selected for nominal operating depths of 30 meters, 120 meters, or 300 meters, respectively.

The operating life of the sonobuoy is selectable prior to launch. Operating life is defined as the elapsed time from water entry until cessation of RF transmission, during which the sonobuoy functions continuously and within the specified performance criteria. The three available operating life settings are 1 hour (+20,-0 minutes), 3 hours (+60,-0 minutes), or 8 hours (+4,-0 hours). Operating life is typically terminated by automatic scuttling of the sonobuoy.

The sonobuoy VHF transmitter operates in the frequency band from 136.000 MHz to 173.500 MHz on 99 separate channels. Each Q-53B sonobuoy can operate on any channel frequency, selectable prior to launch.

The AN/SSQ-53D sonobuoy,³ shown in figure 10(b), is a newer DIFAR sonobuoy. By improving the self-noise characteristics, the frequency response of the Q-53D has been extended down to 5 Hz.

The specifications of the Q-53B and Q-53D buoys make them suitable as elements of a sonobuoy array. The directivity of the DIFAR sensor presents the opportunity to enhance overall array gain by beamforming the directed output of the individual array elements. This would increase the array gain, G , by the average directivity index of the DIFAR sensor. However, the relatively low quality of the cosine and sine data compared to the omni data will limit the contribution of the directional sensor at low frequencies. The DIFAR sensors, being gradient hydrophones, are more sensitive to noise terms introduced by strumming and vertical motion. This is in fact recognized in the Q-53B and Q-53D specifications where considerably worse performance in the DIFAR channels is tolerated.

The availability of the DIFAR information can be exploited to determine the gross orientation of the array prior to the beamforming stage. Near-field orientation uses one or more DIFAR sonobuoys within the array to determine the bearings from which the AEL signals are emanating. This is by far the most practical, robust, and accurate approach to array orientation.

Performing DIFAR processing on a time segment of the DIFAR composite signal containing a received AEL ping will yield a bearing relative to magnetic north from the DIFAR phone to the AEL projector. The desired orientation angle may be derived from this bearing and the pinger-defined array coordinates.

The Q-53 specifications provide for indications of a target's magnetic bearing to be accurate to within ± 10 degrees. Accuracy of the orientation angle can be improved by forming an average of orientation angles derived from the indicated bearings to each AEL projector from each of several DIFAR sensors.

A major disadvantage in selecting the DIFAR sonobuoy for use in arrays is the 2400-Hz low-pass cutoff frequency of the Q-53 frequency response. The confined bandwidth is a direct consequence of the requirement to frequency-multiplex the DIFAR data about the 15-kHz phase pilot. If the ranging signal to be used for hydrophone localization is to be compatible with the DIFAR sonobuoy, the restricted frequency response of the Q-53 severely limits the useful bandwidth of the AEL signal.

Nonetheless, the economies of scale associated with present mass production of the Q-53 result in an inexpensive and readily available sonobuoy for which the following AEL system design will be based.

4.3 MULTIELEMENT SONOBUOYS

A sonobuoy with many widely spaced elements offers the potential for even greater array gain. Particularly desirable is a buoy which, in itself, comprises a vertical line array. Many such buoys deployed as a group would form an extremely sensitive three-dimensional array of line arrays.

Several classes of multihydrophone sonobuoys have been developed in recent years. The problem with most of these is that the hydrophone outputs are beamformed at the buoy to steer the array response in some predetermined direction. The individual hydrophone outputs are not recoverable from the summed signal transmitted from the buoy.

³Military Specification, Sonobuoy AN/SSQ-53D, draft MIL-S-81487E(AS), Naval Air Systems Command, Washington, D.C. 20361-0001, 11 June 1985.

The VHF telemetry bandwidth into which the hydrophone signals of a given sonobuoy may be realistically multiplexed is limited to about 50 kHz. Each buoy could transmit its multiplexed digital data stream over its assigned RF using a simple modulation technique.

As the number of phones per buoy increases, it becomes economical to simplify the AEL to reduce the required telemetry-data bandwidth, recorded-data bandwidth, processing complexity, and cost. Ideally, the data bandwidth should be limited only to the frequencies of interest and not be burdened with the additional bandwidth required for a localizing signal. A line sensor designed from scratch could use in-buoy A/D conversion of the low-frequency-data band.

A line of low-frequency-data sensors could be augmented with at least three reference sensors designed specifically for the detection of some robust AEL signal. The reference sensors would be dedicated to receiving the robust AEL signal and would perform the detection in situ, inserting a detection flag into the digital data stream transmitted to the receiver.

A simple two-element sonobuoy is another promising array element. The output of the two hydrophones would have opposite polarity and would be electrically summed and conventionally telemetered to the aircraft. The spacing of the dipole phones would explicit the known arrival structure of far-field sources.

While the prospect of a multielement sonobuoy is enticing, the AEL system considered in the following sections will focus on existing sonobuoys, particularly the type Q-53.

5.0 REQUIRED AEL ACCURACY

5.1 ACCURACY OF HORIZONTAL ESTIMATION

The hydrophones of a sonobuoy array collectively populate a geometry best described as a horizontal thin disk. As such, beams are steered at or near edgefire, such that the main-response axis is in the horizontal plane of the array or at small elevation angles away from the horizontal.

In beamforming, the delays, τ_j , applied to the output of the hydrophone elements are functions of the array-element-location coordinates. If an estimated array-element location contains some rms horizontal positional error, σ_{xy} , the delay applied to that element when forming a beam will contain an rms phase error, σ_ϕ , which is related to the rms horizontal positional error by

$$\sigma_\phi = \frac{2\pi}{\lambda} \sigma_{xy} . \quad (12)$$

Steinberg (1976) derives the fractional loss in gain due to rms phase errors, which is the actual main-response axis gain, G , relative to the error-free main-response axis gain, G_0 , as

$$\frac{G}{G_0} = \exp [-\sigma_\phi^2] . \quad (13)$$

This relationship is graphically illustrated in figure 12.

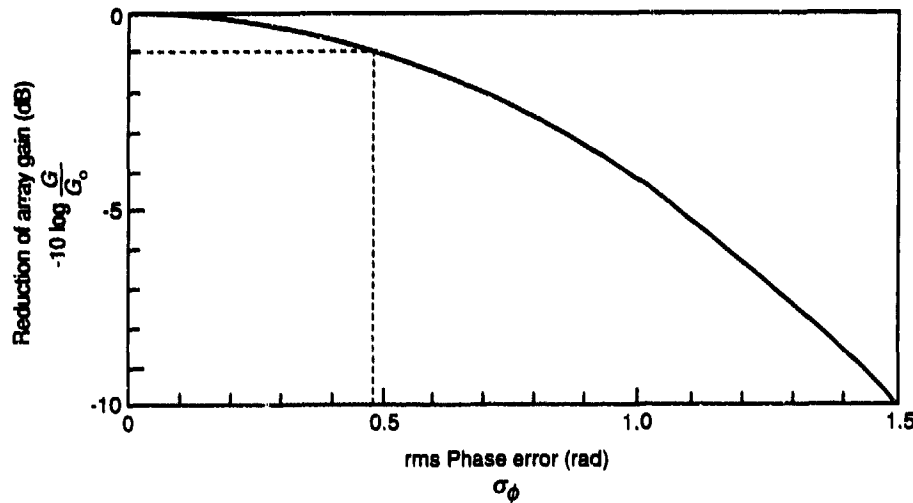


Figure 12. Fractional loss as function of AEL errors.

A 1-dB fractional loss in gain due to element-localization error is generally considered to be the maximum acceptable (Steinberg, 1976). By equation (13), a 1-dB loss would result from an rms phase error of slightly less than 0.5 radian. The loss grows rapidly as the phase error grows. For example, a 1.0-radian rms phase error results in a 4.3-dB loss and a 1.5 radian rms phase error will produce a 10-dB loss.

Based on the maximum acceptable fractional loss in gain, $G/G_0 = 1 \text{ dB}$, the conventional tolerance on array-element location, expressed as a function of acoustic signal wavelength, is obtained from equation (12) as

$$\sigma_{xy} \leq \frac{\lambda}{4\pi} \approx \frac{\lambda}{10} . \quad (14)$$

To satisfy the previously stated goal of detecting acoustic signals in the band up to 150 Hz, the AEL system error budget constraint in the horizontal plane is

$$\begin{aligned} \sigma_{xy} &\leq \frac{\lambda_{\min}}{10} \\ &\leq 1 \text{ meter} . \end{aligned} \quad (15)$$

Range-measurement errors are expected to display Gaussian behavior since they are the result of round-off errors, quantization, ambient noise, and element motion occurring between range measurements. Redundant range measurements will permit estimating array-element locations in some least squares sense, allowing the array geometry to be computed by minimizing the residual errors from an overdetermined system of equations. Gaussian range-measurement errors are, therefore, statistically reduced.

However, if the major source of error is non-Gaussian, the allowable rms range-measurement error should be small enough so that the 1-meter-error constraint on σ_{xy} is satisfied. Non-Gaussian rms range-measurement error is likely to occur if, for example, the dominant error component results from inadequate correction of sound-ray refraction of the ranging signal.

As evidenced by the GDOP example in figure 4, the rms errors in a horizontal-position estimate may have greater magnitude than the rms errors of the ranging measurements. The extent of this error depends upon the trilateration angle θ_{tr} formed by the two range-measurement rays (Lowenstein and Mudie, 1967),

$$\sigma'_{xy} = \frac{\sqrt{2}}{\sin \theta_{tr}} dr_{xy} . \quad (16)$$

Note that the rms error term resulting here from only two AEL references is distinguished with a prime symbol.

With four AEL projectors available, there are six possible combinations of two AEL reference points with which two-dimensional trilateration may be performed. For now, disregard the many optimization procedures that may be applied to these redundant measurements, and instead consider the centroid of only the three "best" AEL combinations. Since σ'_{xy} are rms values, the uncertainty in the horizontal position of the centroid is

$$\sigma_{xy} = \frac{\sigma'_{xy}}{\sqrt{3}} . \quad (17)$$

For array geometries similar to that of figure 5(a), it is reasonable to expect the three best AEL combinations to produce trilateration angles, each of which are within $\theta_{tr} = 90 \pm 30$ degrees. Using $\sin \theta_{tr} = \sin(60^\circ) = \sin(120^\circ)$ and combining equations (15), (16), and (17), we obtain a reasonable horizontal-ranging-measurement goal of

$$\begin{aligned} dr_{xy} &\leq \frac{\sigma'_{xy} \sin \theta_{tr}}{\sqrt{2}} \\ &\leq \frac{\sqrt{3} \sigma_{xy} \sin \theta_{tr}}{\sqrt{2}} \\ &\leq 1.06 \text{ meters} \approx 1 \text{ meter} . \end{aligned} \quad (18)$$

In summary, since range-measurement errors are not likely to be purely Gaussian, rms horizontal range-measurement errors of $dr_{xy} \leq 1$ meter are required to achieve rms horizontal-positional accuracy of $\sigma_{xy} \leq 1$ meter.

5.2 ACCURACY OF VERTICAL ESTIMATION

For beams steered nearly horizontally, rms vertical-positional error, σ_z , is minor in its effect on array directivity index. But vertical-positional errors influence the horizontal-positioning estimates because both are coupled to the range measurement. Furthermore, vertical position uncertainties decrease array gain if the array is steered significantly away from edgefire.

Before investigating these two effects of vertical-positional errors, consider briefly the problem of determining the vertical positions, or relative depths, of the hydrophone elements. The principles of GDOP established earlier lead to the conclusion that the error ellipsoid will have a vertical axis, σ_z , much greater than the horizontal axes, σ_{xy} . This is due to the lack of range measurements outside the horizontal plane of the array and the resulting greater uncertainty of the target-point location in the vertical. Compounding this predicament is the possibility of conjugate solutions for the z -coordinate, mirror images of one another, above and below the plane formed by three AEL projectors. These problems of

hydrophone depth estimation are addressed by using the surface-reflected path of the ranging signal. Reliable depth estimation is dependent on the accurate characterization of the SSP and the correct evaluation of the multipath ray behavior of the AEL signals. The required accuracy of the vertical position is established here based on the demands of the coupling effect and vertical-beam steering.

Coupling of the horizontal component of range measurements to the presumed vertical component has previously been considered with respect to a bottom-moored, horizontal, thin-disk array. The sonobuoy-array coupling error is very similar. Figure 13 is a schematic representation of an AEL projector and a hydrophone element in the array.

The two transducers are separated by a horizontal distance, r_{xy} , and by a vertical separation, r_z . The range distance between the two points is r where

$$r_{xy}^2 = r^2 - r_z^2. \quad (19)$$

Assume now that we lack knowledge of the true vertical separation between the buoys and that we erroneously assume that the vertical separation is $r_z + dr_z$. Using the measured range, r , we would compute an apparent horizontal separation, $r_{xy} - dr_{xy}$, equal to

$$(r_{xy} - dr_{xy})^2 = r^2 - (r_z + dr_z)^2. \quad (20)$$

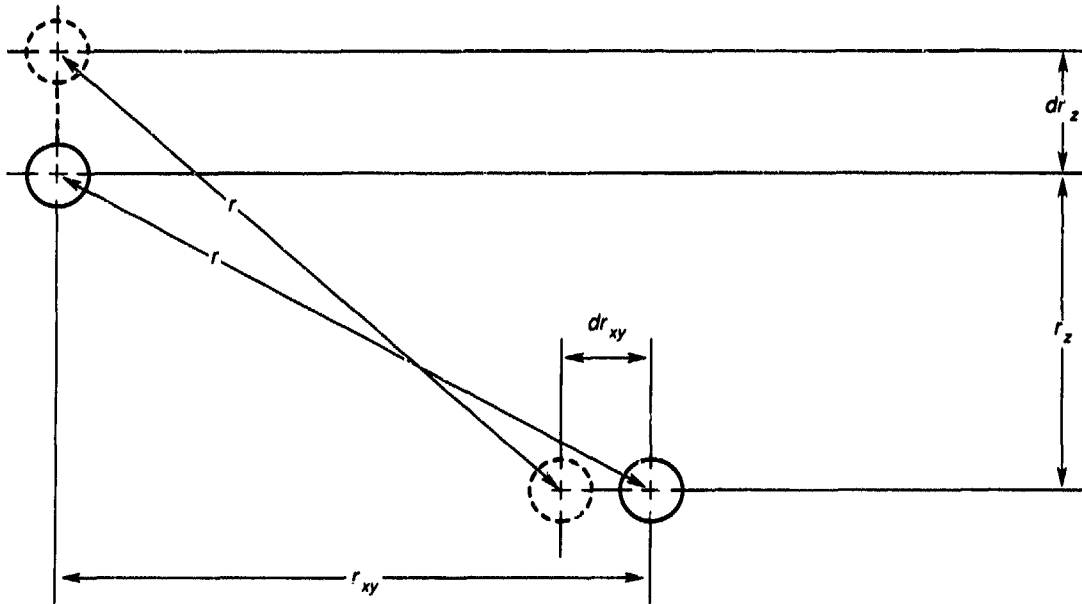


Figure 13. Coupling schematic.

The vertical error, dr_z , may be expressed in terms of the horizontal uncertainty, dr_{xy} , as

$$dr_z = -r_z + \sqrt{r_z^2 + 2r_{xy}dr_{xy} - (dr_{xy})^2}. \quad (21)$$

It has been previously established that the maximum tolerable rms error in the horizontal positioning of the hydrophone elements is $\sigma_{xy} \leq 1$ meter. It has also been established that a horizontal error in our

range measurement of $dr_{xy} \leq 1$ meter will satisfy the tolerance of the horizontal-positional error. The following table shows the allowable vertical uncertainty as a function of the horizontal and vertical separations.

Table 1. Vertical ranging accuracy, dr_z , required to maintain $dr_{xy} = 1$ -meter horizontal ranging accuracy.

		$r_{xy} = \text{horizontal separation (m)}$		
		100	1500	3000
$r_z =$	0	14.1	54.8	77.5
vertical separation (meters)	15	5.6	41.8	63.9
	30	3.2	32.4	53.1
	60	1.6	21.2	38.0
	300	0.3	5.0	9.9

The table shows that for an AEL projector in the plane of the array, vertical uncertainties on the order of 14 meters can be tolerated. The Q-53 sonobuoy specifications allow the manufacturer a ± 10 percent margin of error in operating depth. With a nominal operating depth of 300 meters, this margin of error could produce vertical separations of up to 60 meters. Under these conditions, relative element depth uncertainties on the order of only 1.6 meters could be tolerated for proximal range measurements. Should a sonobuoy suffer deployment problems and become entangled near the ocean surface, the vertical separation would be about 300 meters. In this case, vertical accuracy becomes critical to achieving the required horizontal accuracy. These two extreme cases are rare. An rms vertical-positioning error of $\sigma_z \leq 6$ meters will satisfy the requirements imposed by the coupling phenomenon for over 99 percent of statistically possible projector-receiver pairs.

A second way in which vertical-positioning errors can affect array performance is by reducing the directivity index for beams steered out of the plane of the array. For horizontal beams, the vertical coordinate is entirely absent from the beamforming equations. For beams out of the array's plane, however, vertical coordinate uncertainties affect the directivity index only to the extent of the projection of those uncertainties along the direction that the array is steered. Neglecting horizontal position errors, the directivity index is dependent on the beam-steering elevation angle, ψ_{st} , measured from the horizontal, by

$$DI = 10 \log [1 + (M - 1) \exp(-k^2 \sigma_z^2 \sin^2 \psi_{st})], \quad (22)$$

where M is the number of elements in the array and k is the acoustic wave number (i.e., $k = 2\pi/\lambda$).

Measurements have revealed that $\psi = \pm 18$ degrees is the steepest vertical angle experienced by sound rays propagated from long ranges. The steepest angles occur at the axes of the sound channel such as that depicted in figure 7. In practice, there is no need to steer a beam greater than $\psi_{st} = \pm 15$ degrees since the deep operating depth of a sonobuoy array is well above the sound-channel axis. Combining this angle with the shortest and most demanding acoustic wavelength of interest, $\lambda = 10$ m, and letting a $DI_0 - DI = 1$ -dB fractional loss in gain be the tolerance, the maximum tolerable rms vertical error is computed to be $\sigma_z = 3.06$ meters for an $M = 16$ -element array and $\sigma_z = 2.97$ meters for an $M = 90$ -element array.

In summary, the desire to steer beams away from edgefire by up to $\psi_{st} = \pm 15$ degrees demands that the relative rms vertical-positioning error be

$$\sigma_z \leq 3 \text{ meters} . \quad (23)$$

This requirement is twice as stringent as that required to avoid severe coupling of vertical-localization errors with the horizontal-position estimates, and therefore, dictates the required vertical-estimation accuracy.

6.0 AEL ALGORITHMS

6.1 DATA STRUCTURES

Ping propagation time is the amount of time required for the AEL signal to propagate from a source projector to a receiving hydrophone. The ping propagation time, or simply delay, from AEL buoy i to receiving buoy j will be denoted τ_{ijk} .

The indices i , j , and k form the basis of data structures required for the storage and processing of range measurements.

The subscript i is the AEL index and may assume an integer value between 1 and m , where m is the number of active AEL projectors present in the array.

The subscript j is the receiver index and takes integer values ranging from 1 to 99 since there are 99 radio frequencies for sonobuoy use. The receiver index j of a given sonobuoy corresponds to its RF channel number.

Two functions relate the AEL index to the receiver index. The AEL function, $AEL()$, takes as its argument a receiver index and, if that receiver RF is assigned to an AEL sonobuoy, this function returns the corresponding AEL index. If the argument is not an AEL buoy assignment, the result is zero. The RF function, $RF()$, is the inverse of the AEL function, so that

$$RF(i) = j \Leftrightarrow AEL(j) = i . \quad (24)$$

The subscript k is the path index and has the value $k = 1$ if the direct path is under consideration or $k = 2$ for the surface-reflected path.

The delay, $\tau_{3,27,1}$, is the direct path from AEL unit $i = 3$ to the receiving buoy assigned to RF channel $j = 27$. Note that if $\tau_{3,27,1} = 0$, then RF channel 27 must be assigned to AEL unit #3 and $RF(3) = 27$ and $AEL(27) = 3$. In this case, the delay, $\tau_{3,27,2}$, would be a measure of the round-trip propagation time from AEL unit #3 to the sea surface.

Associated with every delay, τ_{ijk} , is a time tag, t_{ijk} , logging the absolute time at which receiver j begins to be impinged upon by the AEL signal emanating from AEL unit i . Since individual delays, τ_{ijk} , are asynchronously measured, time tags are useful for identifying the relative ages of individual ranging measurements. The time tags play a large role, therefore, in the weighting of redundant measurements based on temporal relevance.

The propagation-time measurements, τ_{ijk} , are converted to straight-line direct and surface-reflected range measurements, r_{ijk} .

6.2 REFRACTION AND SOUND SPEED CORRECTIONS

Given an SSP inferred from a measured temperature profile, conversion of each delay measurement to a geometrically linear range measurement is desired. The linear range measurement obtained from surface-reflected propagation paths is actually the range from the receiver to the image above the sea surface of the projector as shown in figure 9.

An algorithm which essentially performs the inverse function of ray tracing is necessary. The general problem of finding the correct relationship between travel times of sound and the slant range has been addressed, where sound speed is assumed to be a function of depth only (Officer, 1958; Eby, 1967; and Thorp, 1965).

The SSP is approximated by a function composed of a finite number of linear segments, each of which can be integrated exactly. This effectively divides the water column into discrete layers, each having a constant sound-speed gradient described by equation (5).

Such approximations may alternatively be used to directly produce the depth and horizontal range, given both the direct and surface-reflected delays.

6.3 APPROACHES

Delay measurements are made asynchronously if the measurement system performs one delay measurement at a time or if the AEL signal is a pulsed signal rather than a continuous signal. With asynchronously measured data, some measurements are inherently older than others. An effective way of dealing with this temporal disparity is to apply the AEL algorithm to data that are somewhat delayed from the actual time series on which delay processing is being performed. For a given τ_{ijk} , there may actually then be several delay measurements held in memory, each uniquely stamped with a time tag. The delay measurements, including one or more in advance of the localization time, may now be spline-fitted and an interpolated value obtained for the exact time for which localization is desired. If implemented prior to the sound-speed correction, this method provides synchronous range estimates to the AEL algorithm.

Consider a simple subset of sonobuoys containing two AEL buoys and one passive buoy as depicted in figure 14.

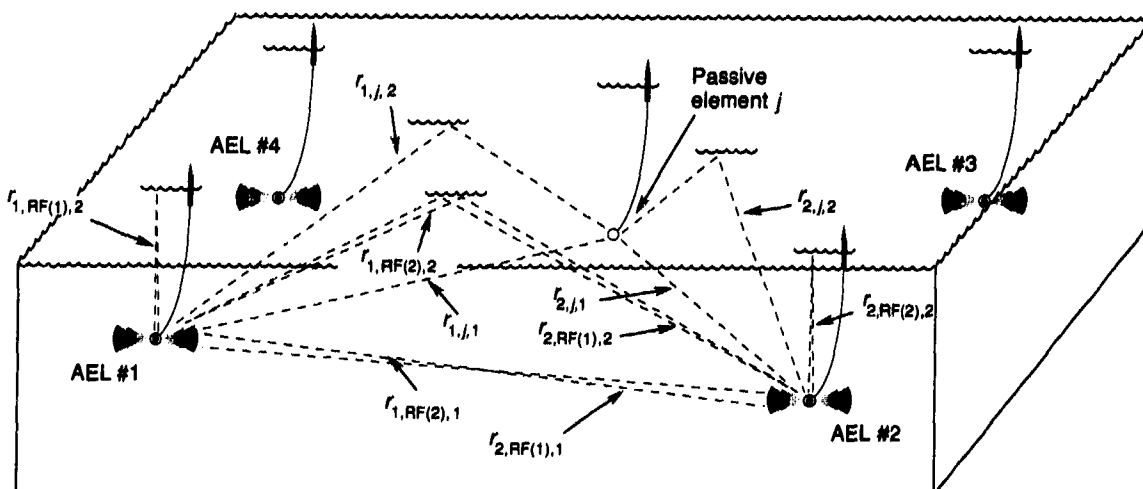


Figure 14. Ranging paths for a subarray.

The three-dimensional localization problem here may be formulated as a problem with six unknowns. The locations on the x' - y' plane formed by the three elements account for three unknowns (by fixing a coordinate system such that the first element is at the origin and the second element is on the x' -axis). The depths of the three elements account for the remaining three unknowns.

Since the paths between the two AEL elements may be independently measured in both directions, a weighted-average measurement,

$$r_{1,RF(2),k} = r_{2,RF(1),k} = wr_{1,RF(2),k} + (1-w)r_{2,RF(1),k}, \quad (25)$$

may be used. Six independent knowns exist in the form of three interelement direct-path lengths, $r_{1,RF(2),1}$, $r_{1,J,1}$, $r_{2,J,1}$, and three interelement surface-reflected-path lengths, $r_{1,RF(2),2}$, $r_{1,J,2}$, $r_{2,J,2}$.

Two solutions are obtained, the true solution and an image of the true solution:

$$x'_{RF(1)} = 0 \quad (26)$$

$$y'_{RF(1)} = 0 \quad (27)$$

$$x'_{RF(2)} = r_{1,RF(2),1} \quad (28)$$

$$y'_{RF(2)} = 0 \quad (29)$$

$$x'_{J} = (r_{1,RF(2),1}^2 + r_{1,J,1}^2 - r_{2,J,1}^2) / 2r_{1,RF(2),1} \quad (30)$$

$$y'_{J} = \pm \sqrt{r_{1,J,1}^2 - x'_{J}^2}. \quad (31)$$

Since the interelement distance measurements will inevitably contain some error, four AEL projectors are normally used within an array. The resulting localization problem is overdetermined, and an AEL algorithm which minimizes the residual error is desired.

The original approach to the error-minimization AEL problem involved the method of least squares. Solutions would be obtained iteratively by initially estimating the positions in two dimensions, neglecting depth, and then dithering the spatial coordinates until the total error of the overdetermined system of trilateration equations was minimized. The error function being minimized is not quadratic, but of higher degree, and possesses numerous relative minima toward which a solution might converge. Initial estimates afforded by AEL-ranging data should be accurate enough, however, to allow reliable convergence to the statistically desired absolute minimum solution.

A realtime approach which estimated element positions by obtaining the weighted centroid of all redundant trilateration solutions was computationally efficient and shown to be accurate with both real and simulated data. The individual solutions were weighted according to the relative consistency of range measurements used and according to GDOP considerations.

Another way to approach the localization problem makes use of a recursive Kalman-filter formulation. Here again, an initial position estimate is used. Each new ranging measurement becomes an update to the estimate toward the direction of minimum variance (Cheung, 1978).

An approach recently implemented at Lockheed is based on techniques developed for drifting acoustic arrays in the arctic. For use with potentially contaminated data, this approach, identified here as the "Duckworth method," appears to be the most robust. Using a combination L_1/L_2 -norm overdetermined nonlinear trilateration equation solver, the method extracts the maximum amount of information possible from data containing errors. The L_2 is a least-squares error norm which tends to spread the fitting error across all data values. The L_1 , or least absolute-value norm, is used for the solution of the overdetermined trilateration equations. Contrary to the properties of L_2 , the L_1 solution solves an overdetermined system so that a number of reliable equations equal to the number of parameters to be estimated are selected and solved exactly. This core of the most consistent equations with no fitting error then exposes unreliable data values through their large residual errors. These bad equations may then be eliminated if their residuals are deemed too large. If the remaining data, including that of the core equations, are assumed to have Gaussian-distributed error, the reduced equation set is subjected to the L_2 least-squares method (Duckworth, 1987).

6.4 DEPTH ESTIMATION

All of the recently implemented AEL algorithms attempt to initially estimate the depth, or z -coordinate, of the array elements. This stage of processing makes use of both the direct and surface-reflected paths, and is critically dependent upon the SSP.

Depth of the AEL sonobuoy hydrophone is measured using the surface-reflected path from the AEL transducer to the AEL hydrophone. This technique produces accurate measurements since the vertical surface-reflected path is perpendicular to density stratification in the water column. Snell's Law tells us that errors due to refraction are negligible. Simple integration over the SSP for the vertical round-trip path will therefore yield the desired self-sounding depth measurement.

The self-sounding measurement is made by autocorrelating the time series from AEL sonobuoy i to obtain $\tau_{i,RF(i),2}$.

A solution for the depths of the three elements in figure 14 is obtained by applying the law of cosines to the geometry of the problem to obtain three independent equations with three unknowns (Rice, 1990). The trigonometric functions are eliminated and the depths of the elements are expressed in terms of the r_{ijk} measurements:

$$z_{RF(1)} = \frac{1}{2} \sqrt{(r_{1,RF(2),2}^2 - r_{1,RF(2),1}^2)(r_{1,J,2}^2 - r_{1,J,1}^2) / (r_{2,J,2}^2 - r_{2,J,1}^2)} \quad (32)$$

$$z_{RF(2)} = \frac{1}{2} \sqrt{(r_{2,J,2}^2 - r_{2,J,1}^2)(r_{1,RF(2),2}^2 - r_{1,RF(2),1}^2) / (r_{1,J,2}^2 - r_{1,J,1}^2)} \quad (33)$$

$$z_J = \frac{1}{2} \sqrt{(r_{1,J,2}^2 - r_{1,J,1}^2)(r_{2,J,2}^2 - r_{2,J,1}^2) / (r_{1,RF(2),2}^2 - r_{1,RF(2),1}^2)} \quad (34)$$

Alternatively, if the self-sounding measurement of the AEL elements is used, the depths are solved with

$$z_1 = \frac{1}{2} r_{1,RF(1),2} \quad (35)$$

$$z_2 = \frac{1}{2} r_{2,RF(2),2} \quad (36)$$

$$z_j = \frac{r_{1,j,2}^2 - r_{1,j,1}^2}{2z_1} = \frac{r_{2,j,2}^2 - r_{2,j,1}^2}{2z_2} . \quad (37)$$

Observe that minor corrections to the SSP may be possible due to the availability of these redundant equations. Highly reliable depth estimates for the AEL elements are first obtained using equations (35) and (36). Then depth estimates for the same AEL elements are recomputed using equation (37), or equations (32)-(34), by alternately letting $j = RF(1)$ and $j = RF(2)$. Any disagreement in the result is due to inconsistency of the assumed SSP. By successively dithering the SSP until these disagreements are reduced, a more realistic propagation model may be obtained.

6.5 HORIZONTAL LOCALIZATION

Once the depth is known for all elements, horizontal localization may be pursued using only the direct-path interelement ranges. Since only the x-y coordinates are required, the horizontal projection of the direct-path range is used.

Even for this simple subset of three buoys, redundant data are available for use by the Duckworth-method L_1/L_2 solver. Each equation involving r_{ijk} may be reformulated as two independent equations.

The raw, intersensor ranges are used to solve the L_1 -norm overdetermined trilateration problem. The first two terms of the Taylor-series expansion of the nonlinear trilateration equations are retained (Aki and Richards, 1980). The linearized equations are now solved by an iterative reweighted least-squares technique to obtain the L_1 solution (Wehner, 1987). Each equation is weighted by the normalized inverse of its fitting error, thereby emphasizing the most consistent equations.

Based on residual-error thresholds, outlier equations are removed. Sufficient equations are retained so that the localization problem remains overdetermined.

The L_2 solution, a nonlinear least-squares fit, is obtained next and a Moore-Penrose generalized inverse is iteratively applied. Unacceptable solutions are identified by the large residual errors.

Instantaneous array geometries determined in the foregoing manner may be further refined by application of a Kalman filter. The temporal sequence of instantaneous array geometries is smoothed and interpolated. Element velocities may be estimated and compared to the physical limits on the forces available to move the sensors. Although not implemented, such filtering operations may ultimately extend the high-frequency range, $f_{\max} = c/\lambda_{\min}$, of the beamforming band. Since position estimates based on the infrequent AEL signals are temporally smoothed and made continuous, AEL errors contributed by relative-drift rate would be virtually eliminated.

7.0 THE AEL SONOBUOY

7.1 AEL SONOBUOY DESIGN CONSTRAINTS

Besides AEL accuracy requirements, many practical constraints influence the design of the AEL sonobuoy and the AEL signal.

The AEL sonobuoy must be constructed such that its size and weight are compatible with standard storage and deployment hardware built into the aircraft. To be contained within the sonobuoy launch package, the AEL signal projector must not exceed 4.25 inches in diameter. Furthermore, the drag characteristics of a deployed AEL sonobuoy must be similar to those of the passive sonobuoys so that ocean currents will not prematurely disperse the buoy field.

The AEL sonobuoy will be constructed using a suspension system similar to that of the passive sonobuoys in the array. For arrays of DIFAR sonobuoys, AEL buoys could be constructed using stock Q-53B's or Q-53D's. By replacing the DIFAR components with AEL components, and compensating for any alteration in drag characteristics, similar relative-drift rates are obtained. By modifying an existing buoy design and retaining its approved launch package, the required air-drop safety qualification of the AEL sonobuoy becomes substantially less stringent.

An omnidirectional hydrophone nearly colocated with the AEL projector is desired (Rice, 1990). Because the depth of the AEL projector is most accurately determined by measuring the "self-sounding" AEL chirp echo reflected from the sea surface, the hydrophone should be located as close to the projector as possible. The omnidirectional hydrophone should also be able to receive pings from the other AEL projectors to accurately establish the AEL reference locations. AEL hydrophone frequency response up to 20 kHz may be desirable to enable localization of the AEL projectors relative to ship-mounted or bottom-moored transponders which normally operate well above the AEL frequency band. Since relatively poor low-frequency response will be tolerated for these hydrophones, it is unlikely that they would be used as array elements for beamforming.

The battery that powers the sonobuoy must sustain a 5-year shelf life and still adequately supply the projector throughout the full 8-hour operating life.

The source level of AEL signals must be sufficient to be detected at a range corresponding to the maximum array aperture of at least 3 kilometers. It must function in environments with ambient noise as great as that associated with sea state 6. The frequency bandwidth of AEL signals is limited to that of the receiving hydrophones. Of the candidate array element sonobuoys, the Q-53B frequency response of 10 to 2400 Hz imposes the most severe bandwidth limitation on the AEL signal design.

Other considerations include simplicity of use, manufacturing tolerances, reliability, cost, and most importantly, signal processing.

The AEL sonobuoys, including the AEL signal format, should be identical. User programmability or adjustment of operating characteristics other than channel assignment, operating depth, and operating life is not desirable. These stipulations are imposed to simplify design, production, inventory, operation, and processing of the AEL sonobuoys. Note that AEL signal designs involving the assignment of orthogonal signals to each of the four AEL sonobuoys is ruled out by these requirements. Orthogonal AEL signals are highly noncorrelative with respect to one another and, by virtue of the use of a distinct matched filter for each AEL sonobuoy, would eliminate confusion in determining the origin of received AEL signals at a given hydrophone. Previous implementations of AEL systems have employed orthogonal AEL signals. However, the complexity and cost of the expendable AEL hardware can be substantially reduced by using a single AEL signal format. Mechanisms for associating received signals with the responsible AEL buoy

can be provided within the AEL sonobuoy RF transmission, thereby providing the benefits of signal identification and a simplified AEL system design.

7.2 THE AEL RANGING SIGNAL

The available operating frequency range of 10 to 2400 Hz is much lower than would normally be chosen for this type of AEL system and imposes a severe bandwidth limitation on the ranging signal. Nevertheless, it is within this limited band that the AEL signal must be designed.

Small low-Q transducers operating in the available frequency band are extremely difficult to develop. To limit power consumption, continuous ranging signals are rejected in favor of pulsed signals. The allowable time between pulses is determined by the required AEL accuracy and relative-sonobuoy drift.

Propagation time from the AEL projector to a receiver is measured by cross-correlating the projected pulse within the time series, $x_{RF(j)}(t)$, with the audio output of the receiving hydrophone element, $x_j(t)$. Let the onset of the acoustic transmission of the AEL signal occur at time, t_0 , the propagation time across the entire array aperture be denoted as T_{ar} , and the duration of the AEL signal be T_{sig} . The cross-correlation function for the observation time $T_{ar} + T_{sig}$,

$$R_{ij}(\tau) = \int_{t_0}^{t_0 + T_{ar} + T_{sig}} x_{RF(j)}(t) x_j(t + \tau) dt, \quad (38)$$

will contain peaks representative of the temporal arrival structure of multipath propagation. $R_{ij}(\tau)$ gives a measure of the degree of similarity between the time signal, $x_{RF(j)}(t)$, and a displaced version of the time signal, $x_j(t)$, as a function of the time displacement τ . The peaks of the cross-correlation function, therefore, yield the propagation times of the dominant paths. Consider a noiseless, synchronized replica, $s_i(t)$, of the projected AEL signal. For times before and after projection of the AEL signal, the replica is zero:

$$\begin{aligned} s_i(t) &= 0, \text{ if } t < t_0 \\ &\neq 0, \text{ if } t_0 \leq t \leq t_0 + T_{sig} \\ &= 0, \text{ if } t > t_0 + T_{sig} \end{aligned} \quad (39)$$

If $s_i(t)$ is substituted for $x_{RF(j)}(t)$ in equation (38), spurious correlation peaks due to received AEL signals present in $x_{RF(j)}(t)$ are avoided.

The correlator may alternatively be implemented as a matched filter, providing optimal performance. The impulse response, $h_i(t)$, of $s_i(t)$ is used to obtain the temporal response of the filter to the received signal $x_j(t)$,

$$y_{ij}(t) = \int_0^{T_{sig}} h_i(\tau) x_j(t - \tau) d\tau. \quad (40)$$

Selection of signal waveform is restricted to pulsed signals due to battery limitations. Factors such as signal covertness, measurement resolution, processing ease, and required wet-end hardware must also be weighed.

Some applications of a sonobuoy array would benefit from covert operation of the localization system. A ranging signal that would accommodate such a requirement would be composed of band-limited

pseudorandom noise. The value of a covert AEL signal is questionable, however. Covertness of the array is compromised by the loud splashdown of the sonobuoys during deployment and is further relinquished by the loitering behavior of the monitoring aircraft. For these reasons, and since the projection of random noise signals is extremely inefficient, the covertness constraint is discarded.

The resolution of the propagation-time measurement is physically manifested as the width of the correlation peak. The ideal shape for the matched-filter output would be the impulse, thereby providing maximum resolution of the propagation measurement. A quality measure of candidate ranging-signal waveforms is the determination of how impulse-like the autocorrelation function of the replica $s(t)$ is. An equivalent quality measure is the comparison of the spectrum of the autocorrelation function with the spectrum of an impulse. The resulting factor is the effective bandwidth, β_{eff} , of the waveform.

While the spectrum of an impulse is ubiquitous and flat at *all* frequencies, the band available for the AEL signal will allow only a rectangular spectrum limited to the Q-53 frequency response. The inverse Fourier transform of a rectangular function is a sinc function, where the width of the pulse is the reciprocal of the bandwidth.

Consider a waveform commonly used in radar applications (Wehner, 1987). The linear frequency-modulated pulse, also called a chirp, is expressed in complex form as

$$s(t) = \text{rect} \left[\frac{t}{T_{\text{sig}}} \right] \exp [j2\pi(\bar{f}t + \frac{1}{2}Kt^2)], \quad (41)$$

where T_{sig} is the pulse duration, \bar{f} is the center frequency or carrier, K is the chirp rate or frequency sweep rate, and

$$\begin{aligned} \text{rect} \left[\frac{t}{T_{\text{sig}}} \right] &= 1, \quad \text{if } \left| \frac{t}{T_{\text{sig}}} \right| < \frac{1}{2} \\ &= 0, \quad \text{if } \left| \frac{t}{T_{\text{sig}}} \right| > \frac{1}{2} \end{aligned} \quad (42)$$

During the pulse duration T_{sig} , the instantaneous frequency changes from $\bar{f} - \frac{1}{2}KT_{\text{sig}}$ to $\bar{f} + \frac{1}{2}KT_{\text{sig}}$. This frequency sweep is symbolized by Δ .

When the chirp bandwidth β_{Δ} is large, the autocorrelation function of the chirp resembles a sinc function with width inversely proportional to β_{Δ} . Pulse compression inversely proportional to the bandwidth of the chirp is achieved (Klauder, Price, Darlington, and Albersheim, 1984).

With respect to the design of the projector, a chirp waveform is a practical choice for the ranging signal. Driving the smooth frequency transition of the linear modulation sweep may be efficiently accomplished. If the mechanical and electrical resonances of the transducer are exhibited at or near the bandcenter of the chirp, maximum efficiency is achieved.

Output power of the projected chirp will be substantially reduced for frequencies away from the resonances. Careful design of the transducer places the resonances near the center of the swept frequency band. Amplitude of the chirp, referenced to the bandcenter, will continuously decrease toward the bandedges.

By virtue of the linearity of the frequency sweep, the response falloff imposed by the transducer will produce a rounded envelope in both the time and frequency domains. This natural windowing of the chirp suppresses the secondary peaks in the sinc-like, matched-filter response. Identification of the main peak is

thereby assured and resolution of neighboring main peaks produced by multipath-signal arrivals is aided. Due to the loss of energy at the skirts of the chirp spectrum, the effective bandwidth is less than the chirp bandwidth, $\beta_{\text{eff}} < \beta_A$, and slight widening of detection peaks out of the matched filter will be suffered.

The AEL signal center frequency should be selected to allow maximum effective bandwidth of the chirp. At the low end of the spectrum, the signal is limited by the allowable size of the transducer. At the high end of the spectrum the limitation is imposed by the bandstop frequency of the Q-53 sonobuoy. The band between 1400 Hz and 2350 Hz is practical.

If, during signal processing, the bandcenter of the AEL band is to be digitally base-banded by quadrature demodulation, special care must be used in determining the chirp center frequency. Computationally efficient quadrature demodulation requires that the sequence of sines and cosines of the bandshift frequency consists only of minus ones, zeroes, and plus ones. These simple integer coefficients result, for the present application, only from a sampling frequency four times the desired bandshift. Recall that the high amplitude 7.5-kHz pilot tone of the composite DIFAR signal is allowed a tolerance of ± 25 Hz (see footnote #3). If this signal survives suppression by the antialiasing filter and should fold into the beamforming frequency regime, contamination of the data would result. If digital quadrature demodulation is intended, frequencies between 1830 and 1920 Hz should not be used as the chirp center frequency. Avoiding these frequencies will protect the 0- to 155-Hz band from possible contamination.

Candidate AEL bands are 1400 to 2260 Hz with $\bar{f} = 1830$ Hz and $\beta_A = 860$ Hz, or 1490 to 2350 Hz with $\bar{f} = 1920$ Hz and $\beta_A = 860$ Hz. If digital quadrature demodulation is not intended, then the entire available bandwidth of $\beta_A = 950$ Hz could be used with bandcenter at $\bar{f} = 1875$ Hz.

For the prototype system developed to validate the AEL concept, a $\beta_A = 800$ -Hz chirp centered at $\bar{f} = 1875$ Hz was selected since it was shown that the DIFAR pilot tones could be adequately suppressed using a carefully designed low-pass filter. Referenced to \bar{f} , the amplitude is down 3 dB at ± 200 Hz and down 12 dB at ± 400 Hz. The amplitude response envelope of the prototype AEL (PAEL) signal is specified according to figure 15. Since the instantaneous frequency of a chirp increases linearly with time, the abscissa may simultaneously describe both parameters. The sound-pressure level constrained by the upper and lower limit curves may, therefore, be read either as a function of instantaneous frequency or time. The effective bandwidth is conservatively declared to be $\beta_{\text{eff}} = 400$ Hz for this windowed waveform.

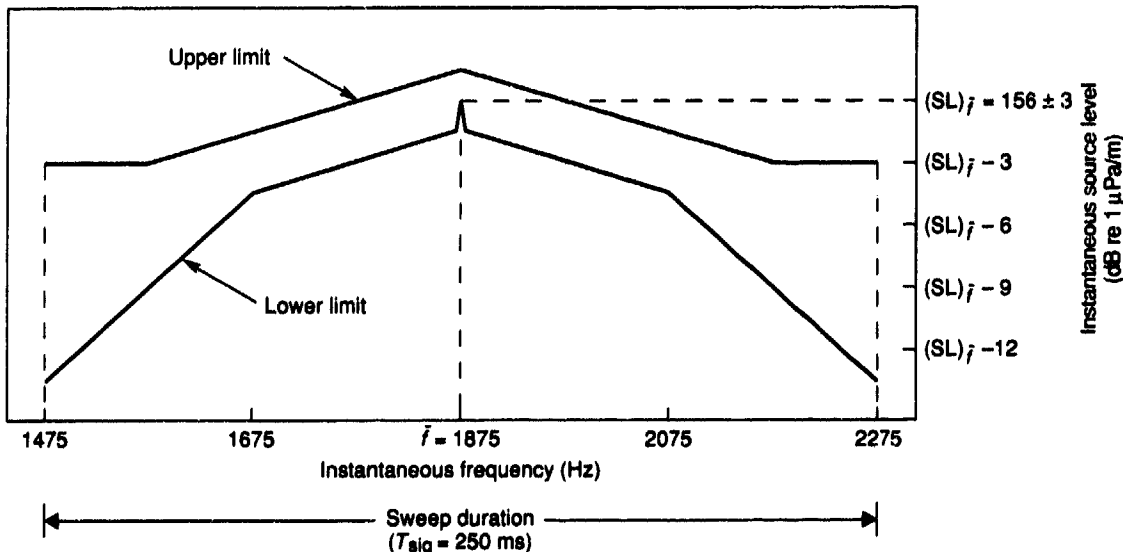


Figure 15. PAEL signal response.

Duration of the chirp is chosen to be $T_{sig} = 250$ ms. This is short enough that interference of simultaneously arriving pings is infrequent, yet sufficient to assure adequate matched-filter processing gain, as will be seen.

Correlation pulsedwidths of $1/\beta_{eff} = 2.5$ ms may be expected from the PAEL signal for (worst) cases where only the middle 400-Hz band of signal responds to the matched filter. By virtue of the additional 400-Hz bandwidth at the skirts of the "effective" AEL signal, the suppressed secondary-peak structure allows excellent resolution of overlapping signal arrivals. Taken alone, the pulsedwidth represents a gross accuracy of 3.75 meters. To attain greater accuracy, it is necessary to operate at a sufficiently high signal-to-noise level to permit interpolation within the peak of the matched-filter output. This is achieved through a combination of matched-filter processing gain and high signal levels.

Signal simulation has shown that interpolation to 1/5 the width of the correlation peak, corresponding to about 0.75-meter ranging accuracy, may be reliably achieved with an SNR at the matched-filter output of $(S/\pi)_{out} = 20$ dB. Subsequent peak-picking algorithms can provide even further accuracy. The SNR following matched-filter processing is the decibel sum of the SNR at the input to the matched filter plus the signal-processing gain afforded by the matched filter itself,

$$(S/\pi)_{out} = (S/\pi)_{in} + PG . \quad (43)$$

Matched filtering is a pulse-compression process whereby the amplitude of the compressed pulse is proportional to the effective time-bandwidth product of the received waveform. Signal-processing gain is the factor by which the SNR at the output of the matched filter is increased over that at the input. Processing gain is dependent on the time-bandwidth product of the waveform by

$$\begin{aligned} PG &= 10 \log [2(T_{sig})_{eff} \beta_{eff}] \\ &= 10 \log [2(0.125s)(400 \text{ Hz})] \\ &\approx 20 \text{ dB} . \end{aligned} \quad (44)$$

Processing gain for a given received signal approaches equation (44) as the received signal waveform begins to resemble the AEL signal replica. A signal-to-noise level of

$$(S/\pi)_{in} = 0 \text{ dB} . \quad (45)$$

at the input of the matched filter is, therefore, adequate.

Required source level of the AEL signal at the center frequency is the sum of the TL due to propagation across the array aperture, in-band noise in sea state 6, minimum SNR prior to signal processing, and a signal-to-noise safety margin of $SM = 13$ dB. Equations (10), (11), and (45) are combined to obtain

$$\begin{aligned}
 SL &= TL + NL + (S/\pi)_{in} + SM \\
 &= TL + NL + (S/\pi)_{out} - PG + SM \\
 &\approx 78 \text{ dB} + 65 \text{ dB} + 20 \text{ dB} - 20 \text{ dB} + 13 \text{ dB} \\
 &\approx 156 \text{ dB} .
 \end{aligned} \tag{46}$$

A chirp signal can be actively generated by driving a voltage-controlled oscillator with a time-varying drive voltage that results in the desired linear frequency ramp. Alternatively, passive chirp generation results from driving a linearly dispersive filter with a very short pulse (Wehner, 1987).

7.3 TRANSMISSION OF THE AEL SIGNAL

Since the sonobuoy array will normally include four AEL sonobuoys, the implementation of an AEL signal-transmission scheme must meet the following minimum criteria:

- A method must be available to associate a given ping with the responsible transmitting AEL sonobuoy.
- Ping interference and the resulting loss of range-measurement data must be minimized. Ping interference occurs whenever a hydrophone is excited by more than one AEL signal simultaneously. A chronological sequence of interference regions of two pings is demonstrated in figure 16. Array elements located in the double-shaded areas are being simultaneously illuminated by both pings. Consecutive ping interferences of signals from the same source buoys at a given receive buoy must particularly be avoided.

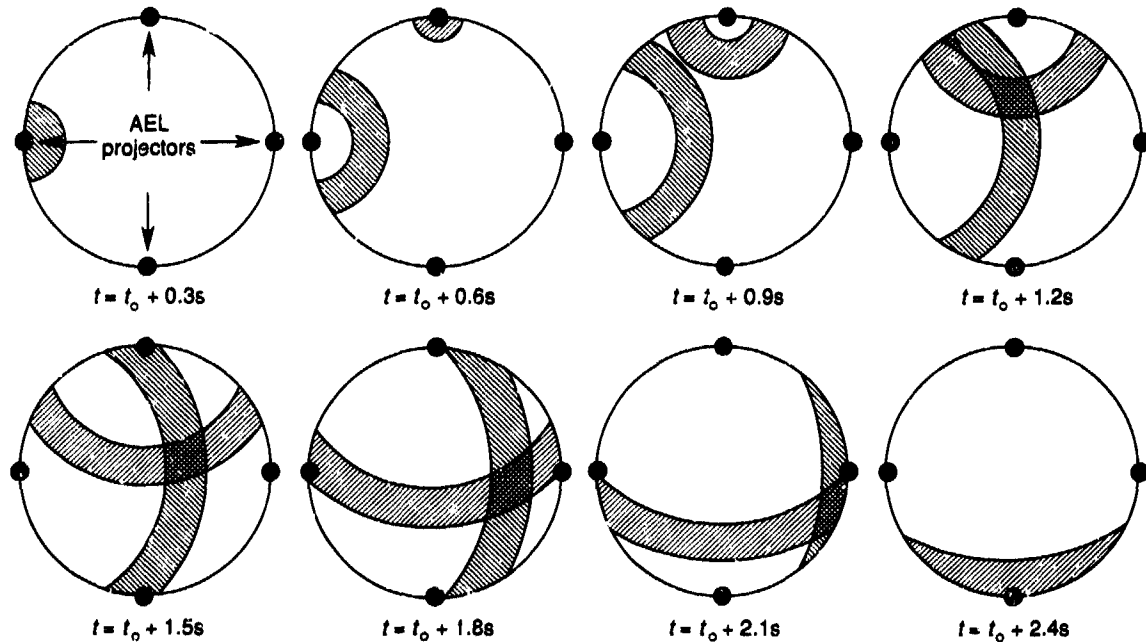


Figure 16. A chronological sequence of interference regions.

Besides the foregoing minimum criteria, the following criteria are desired to reduce buoy manufacturing cost and to simplify buoy operation and data processing:

- c. All AEL sonobuoys should be identical.
- d. The AEL sonobuoy should function independently of the other deployed sonobuoys.
- e. Downlinked commands from the aircraft should be unnecessary.
- f. The synchronization of ping patterns or relative ping phases of the AEL buoys in a given array should be unnecessary.
- g. A start pulse indicating the onset of acoustic transmission of the AEL signal should be present in the AEL sonobuoy data sent to the aircraft via the RF link.
- h. A replica of the acoustically transmitted AEL signal should be delivered to the aircraft via the RF link. This replica should be coincident with the acoustic projection of the AEL signal into the sea to allow cross-correlation of the replica with signals received at the array hydrophones.

Criterion a may be met by implementing the suggestions given by criteria g and h. A high-amplitude start pulse, surrounded by blanked audio, precedes the replica and is provided as a cue that projection of the chirp is imminent. When a start pulse is detected on a channel assigned to an AEL buoy, the airborne-processing equipment may be triggered to set up for a matched-filtering operation. The projected signal waveform may be obtained either by allowing the AEL sonobuoy hydrophone to sense the projected ping, or by blanking the hydrophone signal and substituting an electrically generated replica onto the data line. The latter approach avoids problems that may arise from overloading or clipping the hydrophone located just beneath the AEL-signal projector. Propagation-time-measurement errors caused by variance in the starting frequency from the nominal value are also avoided. Electrical transmission of a replica chirp exactly synchronized with the acoustic transmission will provide the matched filter, $s(t)$. Use of a buoy-generated replica rather than a stored replica avoids the need to tightly specify the tolerances of the chirp waveform.

Following the replica, blanking of the colocated omnidirectional hydrophone must stop to receive the echo of the AEL signal reflected from the sea surface. This reflected signal will allow an accurate self-sounding measurement of the AEL sonobuoy projector/hydrophone depth.

Patterns whereby the AEL signal is transmitted with a fixed period between pings violate criterion b since consecutive interference will occur whenever the time offset between any two ping patterns is less than the time required for sound to propagate through the array. Interference patterns such as that depicted in figure 16 would persist. For a nominal array aperture of 3000 meters, a sound speed of 1500 m/s, and a ping length of 250 ms, this minimum time offset is 2.25 seconds. It is possible to schedule the pings such that the time offset always exceeds 2.25 seconds, but this would require acoustical feedback, downlinked feedback, or phase initialization of the ping cycle prior to deployment (violating criteria d, e, and f, respectively).

To avoid the problem of consecutive ping interferences, the period between pings could vary from buoy to buoy. However, this would require differences in the buoys or initialization of the ping periods prior to deployment (violating criteria c and f, respectively).

Several ping patterns that satisfy the foregoing criteria have been considered. The candidate patterns are all based on the tactic of varying the period between consecutive pings. To maintain the required ranging accuracy, the pseudorandom interping periods for all candidate patterns have expected values of 30 seconds. This nominal ping rate is sufficient to adequately track element motion expected from worst-case relative-drift rates.

To test the relative proficiency of these patterns in meeting criterion b, they were all subjected to simulation analysis to determine the probability of ping interference and consequent lost range measurements. Analysis of ping-interference rates experienced during these extended simulations produced an average data-loss rate and a maximum data-loss rate for each candidate. The average data-loss rates were comparable for all of the ping patterns considered. The worst-case data-loss rates, which proved to be a good indicator of AEL sonobuoys with in-phase patterns, were used to eliminate the majority of candidates.

The AEL sonobuoy ping pattern recommended by this analysis has periods lasting between 25 and 35 seconds between consecutive pings. The random variation of period duration is uniformly distributed across the 25- to 35-second range and is independent of previous periods. A sequence of ping periods (rounded to the nearest second) from a given AEL sonobuoy, for example, could be

..., 28, 34, 29, 30, 35, 34, 26, 29,

Analysis showed that the worst-case data-loss rate would not exceed 6 percent.

Further reduction in the interference rate to below 2 percent is achieved by sweeping down in frequency for alternate chirps from each AEL transducer. If a downswept AEL signal encounters a hydrophone concurrently with an upswept AEL signal, no data loss is suffered since chirps with opposite sweep directions do not correlate. Consistent interference of multiple AEL signals at any array element is thereby excluded.

At the end of the designated life of the AEL sonobuoy, acoustic transmission and RF transmission cease. Scuttling the sonobuoy in this manner prevents interference with freshly seeded AEL sonobuoys.

8.0 EXPERIMENTAL VALIDATION

8.1 THE PAEL SONOBUOY

Based on the foregoing analysis, a specification for a prototype AEL sonobuoy was prepared.⁴ Sonobuoys developed according to this specification were designated PAEL sonobuoys. A quantity of 200 units was desired to validate the buoy design and to evolve the specification of an improved AEL sonobuoy. Array data collected with PAEL sonobuoys would also be used to develop and verify beamforming algorithms.

During the early stages of development of the specification, discussions were held with the two contractors who had Q-53B buoys in current production. One proposed a predominantly digital approach and the use of a transducer developed for another application. The other proposed an analog approach and the use of a modified transducer with a tuning network to extend its response. The specification tolerances were stated as loosely as possible to maximize flexibility in the hardware design and to reduce production costs. Since the transducer appeared to be the highest risk item, it was specified in terms of upper- and lower-limit curves for its response. Tolerances on the signal were kept wide enough to permit an analog implementation. A major concern at this point was to ensure competing bids on these relatively costly buoys. The final specification could be met by either proposed approach.

Both sonobuoy manufacturers were invited to bid on the contract. Since both companies submitted acceptable proposals, the low bidder prevailed. The contract was awarded in 1984 to Magnavox Electronic Systems Company of Fort Wayne, Indiana.

⁴Military Specification, PAEL Sonobuoy (draft), Naval Air Systems Command, Washington, D.C. 20361-0001, November 1984.

Figure 17 is an illustration of a PAEL sonobuoy deployed at the deep operating depth. Although Magnavox had intended to use analog circuitry in much of its design, it soon became evident that a digital implementation was more practical.

It also proved more difficult than anticipated to stretch the transducer response. Magnavox abandoned that approach and began development of a special transducer from scratch. Problems with instability under varying temperature and pressure conditions, unit-to-unit nonrepeatability, and insufficient source level posed significant engineering challenges that had to be overcome.

After 2 years of development, including extensive trial-and-error refinement, a transducer superior to any originally envisioned was produced. Figure 18 is a photograph of a recovered PAEL electronics canister, projector, and omnidirectional hydrophone.

The transducer is a free-flooding cavity constructed of graphite and aluminum. Sea water is forced in and out through two small portholes by alternately expanding and compressing the cavity, creating a Helmholtz resonator. The geometry of the vented cavity is a rigid cylindrical can, with an active element centered within the top and bottom plates. The active elements, ceramic bimorph benders potted in silicone, act in opposition to one another to excite the volume of the cavity. Specific design parameters are company proprietary data and are not disclosed here.

Timing and waveform generation have been digitally implemented, achieving accuracy orders of magnitude superior to the specification. Superimposition of audio blanking, start pulse, and PAEL signal replica onto the omnidirectional-audio signal is depicted in figure 19(a).

Figure 19(b) is the Fourier transform of the rectangularly windowed figure 19(a) time series from $t = -10$ ms to $t = 265$ ms.

8.2 TEST ARRAYS

Extensive ocean testing has been performed using the PAEL sonobuoys. In all cases, arrays were formed consisting of $3 < m < 5$ PAEL sonobuoys and up to $M = 90$ passive sonobuoys. A summary of the experimental arrays is presented as table 2.

Engineering tests, design approval tests, and lot acceptance tests were performed near shore where the sonobuoy telemetry signals could be received by a land-based RF antenna. The excellent results in the lot acceptance tests were in sharp contrast to experience in the early engineering tests. The engineering tests, required due to concern about some of the high technical risk areas, were not pass/fail tests. Intended solely to provide early warning of potential problems, these tests proved extremely useful. Besides the transducer difficulties, other unanticipated failure modes were identified. One change resulting from these tests was incorporated into the Q-53B design.

Subsequent testing in the open ocean required aircraft for deployment and data recording. Most of these experiments included one or more far-field acoustic sources to test the array properties.

8.3 RANGING MEASUREMENTS

The received audio signals are filtered and digitized before matched-filter processing commences. Data volume considerations are nontrivial because of the large number of data channels involved.

Each of the PAEL channels are routed to analog start-pulse detectors where the start pulse preceding the PAEL signal replica is detected. While digital detection of the start pulse is viable, analog start-pulse detection benefits from the availability of start pulses undegraded by antialiasing filters.

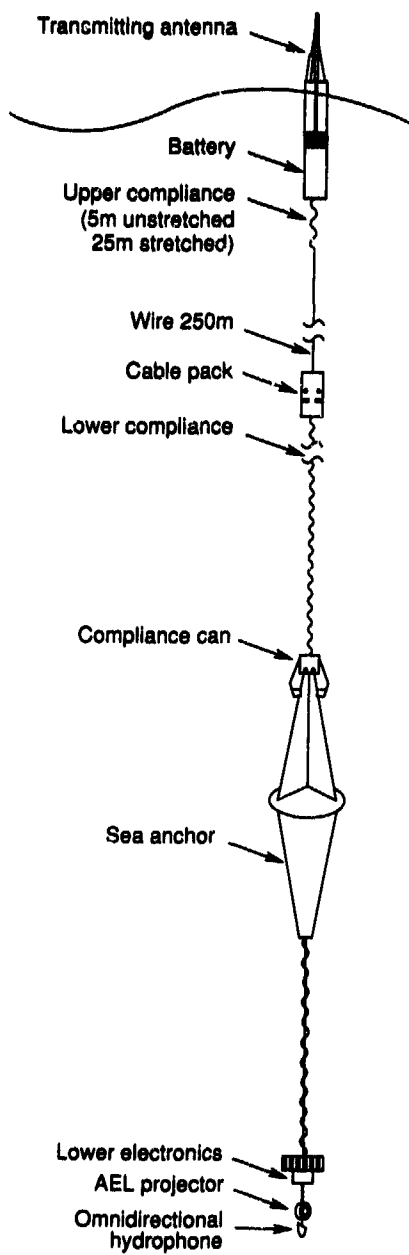


Figure 17. PAEL sonobuoy.



Figure 18. PAEL sonobuoy lower unit.

Each audio channel contains two frequency bands of interest. The beamforming band contains the low-frequency acoustic information in the 5-Hz to 150-Hz range that the beamforming algorithms will require. The AEL band contains the PAEL signals in the 1475-Hz to 2275-Hz range.

At this point, each channel could be split into two subchannels. Analog bandpass filters would preserve the beamforming band on one subchannel and preserve the AEL band on the other subchannel.

To lower the required sampling rate of the AEL band subchannel, analog transformation of the filtered signal to a base-banded complex envelope representation could be performed by multiplying the signal by the sine and cosine of 1875 Hz. The resulting real and imaginary components would then be lowpass filtered with a cutoff frequency just above 400 Hz. This base-banding operation would significantly reduce the volume of data and the corresponding memory requirements by at least 60 percent (5000 samples/s/ch versus 300+900+900 samples/s/ch).

The regrettable tradeoff that must be made to realize this reduction is an increase in analog circuitry and the consequent increase in power consumption and risk of failed components. Although at a much lower sampling frequency, digitization would be required for three times the number of analog channels.

The lower risk approach to the signal conditioning problem is to simply bandpass filter each of the audio channels such that the 5- to 2275-Hz band is preserved. The energy below 5 Hz includes strumming noise from the sonobuoy suspension and a large DC component produced by most of the stock sonobuoy receivers as an indication of sonobuoy RF signal strength. Unnecessary clutter in the 150- to 1475-Hz band could optionally be removed from the signal with a bandstop filter, but the tradeoff of a more complicated filter stage is a larger hardware package and increased phase distortion in the frequency bands of interest.

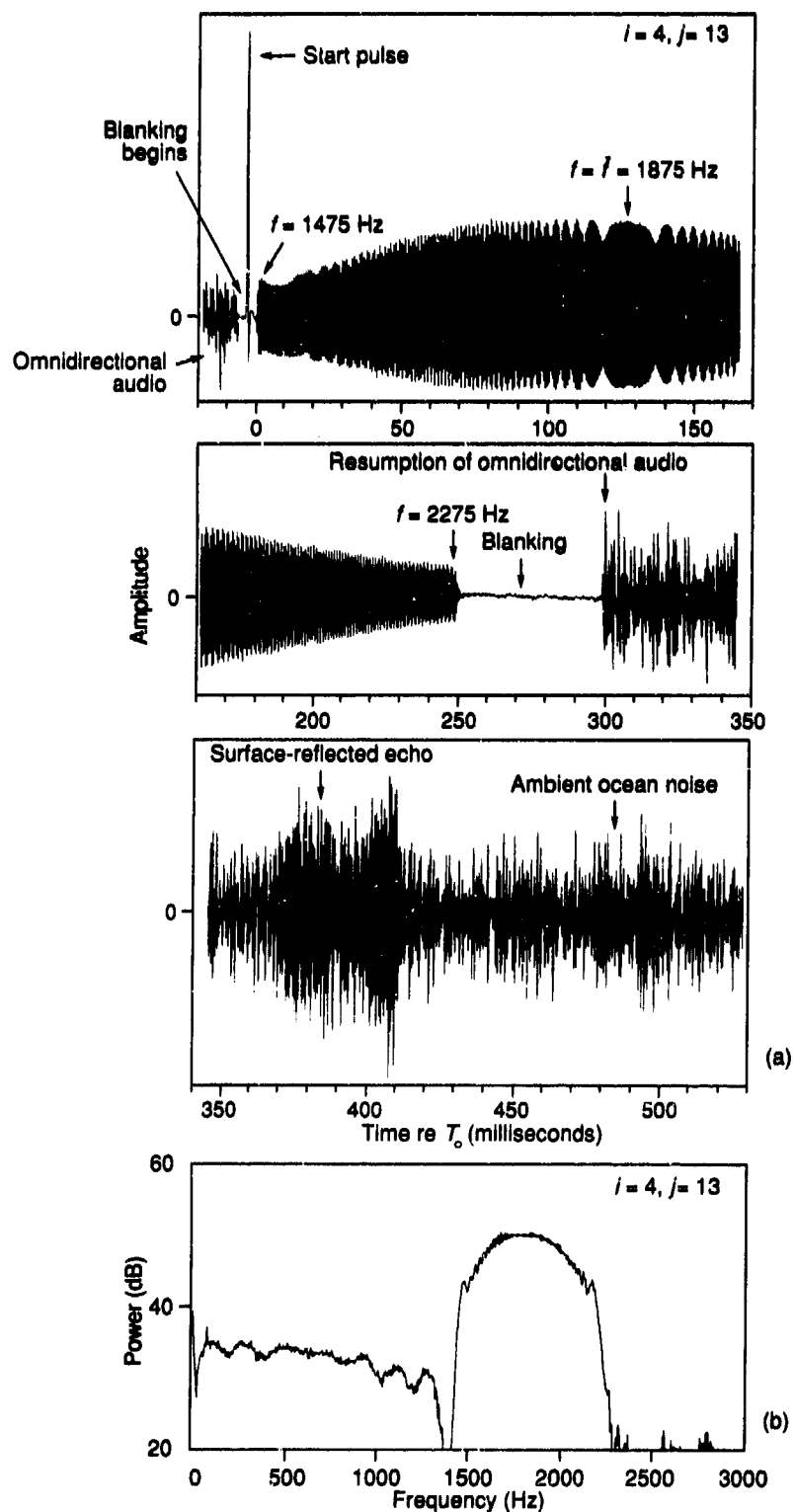


Figure 19. PAEL signal replica.

Table 2. Summary of experimental arrays using PAEL sonobuoys.

Array ID #	Location	Date	<i>m</i> PAELs good/ deployed	<i>M</i> Passive sonobuoys good/type	Operating depth (m)	Array aperture (m)	Notes
31 32	St. Croix	06/25/86 06/27/86	1 / 4 4 / 6	4/53B 5/53B	300 300	2000 1000	engineering tests
41 42	St. Croix	03/18/87 03/20/87	4 / 6 4 / 6	6/53B 6/53B	300 300	2000 2000	engineering tests
51 52	St. Croix	07/24/87 07/26/87	4 / 4 4 / 4	16/53B 16/53B	300 300	2800 2800	design approval test
61	St. Croix	09/02/87	5 / 5	15/53B	300	2500	lot 1 test
71	St. Croix	09/30/87	5 / 5	15/53B	300	2500	lot 2 test
81 82	St. Croix	12/02/87 12/03/87	4 / 4 4 / 4	17/53B 17/53B	300 300	3000 3000	lot 3 acceptance tests
91	North Pacific	08/31/88	3 / 3	11/VLF, 1/53B 10/Swallow floats	300	1000	VLF sonobuoy experiment
101 102 103 104	North Pacific	10/13/88 10/13/88 10/15/88 10/15/88	4 / 4 4 / 4 4 / 4 4 / 4	19/VLF 19/VLF 19/53B 19/53B	120 120 300 300	1400 1400 2800 2800	Outpost Sunrise experiment
121 122	North Pacific	11/09/88 11/09/88	4 / 4 4 / 4	19/VLF 19/53B	120 300	1400 1400	Transit-Ex experiment
131 132 133	North Atlantic	05/24/89 05/24/89 05/24/89	4 / 4 3 / 4 4 / 4	15/53D 14/53D 13/53D, 4/53B	300 300 300	1400 1400 1400	STRAP-Ex experiment
143 144 145	North Atlantic	07/10/89 07/12/89 07/14/89	4 / 6 4 / 4 4 / 5	34/53B 27/53B, 4/41B 39/53B	300 300 300	3000 3000 3000	VAST-I experiment
161 162	West Atlantic	08/11/90 08/11/90	4 / 5 4 / 4	20/53D 20/53D	300 300	1500 1500	NATIVE-I experiment

If ideal lowpass filtering with infinite rolloff at exactly 2275 Hz could be achieved, the sampling theorem would lead us to conclude that our signal is completely defined if sampled at $f_s = 4550$ Hz, or twice the highest frequency contained in the signal. Actual filters do not exhibit steep rolloff without affecting phase linearity of energy in the adjacent passband. To avoid phase distortion in the AEL band, a low-order lowpass filter with gradual rolloff is selected.

The best filtering solution appears to be a highpass filter with cutoff frequency at 5 Hz in series with a gentle lowpass filter with cutoff frequency at 2275 Hz. Following the filtering stage, the data channels are ready for digitization.

The lowest acceptable sample rate is twice the highest frequency at which energy persists in amounts that can be quantized by the A/D converter. Images of unsuppressed spectral energy above $\frac{1}{2}f_s$ will fold

back into the passband, potentially contaminating information in the beamforming and AEL bands. For composite DIFAR signals, suppression of the high-amplitude pilot tone is of particular concern.

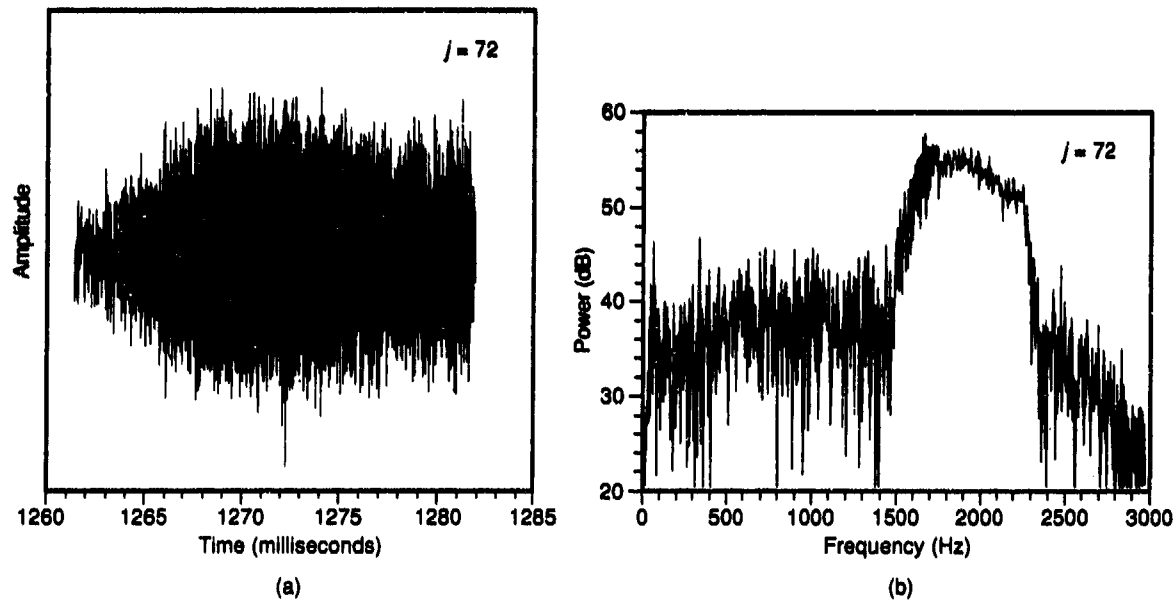


Figure 20. Received PAEL signal at $r = 275$ -meter element.

A sample rate of $f_s = 7500$ Hz has been implemented and used to process a subarray of Array 143. The displayed PAEL signal of figure 19 and the time series of figures 20(a) and 21(a) are realizations of this processing. The time series of figures 20(a) and 21(a) are centered on the direct-path arrival of the PAEL $i = 4$ signal associated with figure 19. Power spectra are given as figures 20(b) and 21(b). Subsequent AEL analysis indicates that receiver $j = 72$ of figure 20 is $r = 275$ meters away from the PAEL transducer and that receiver $j = 29$ of figure 21 is $r = 1710$ meters away.

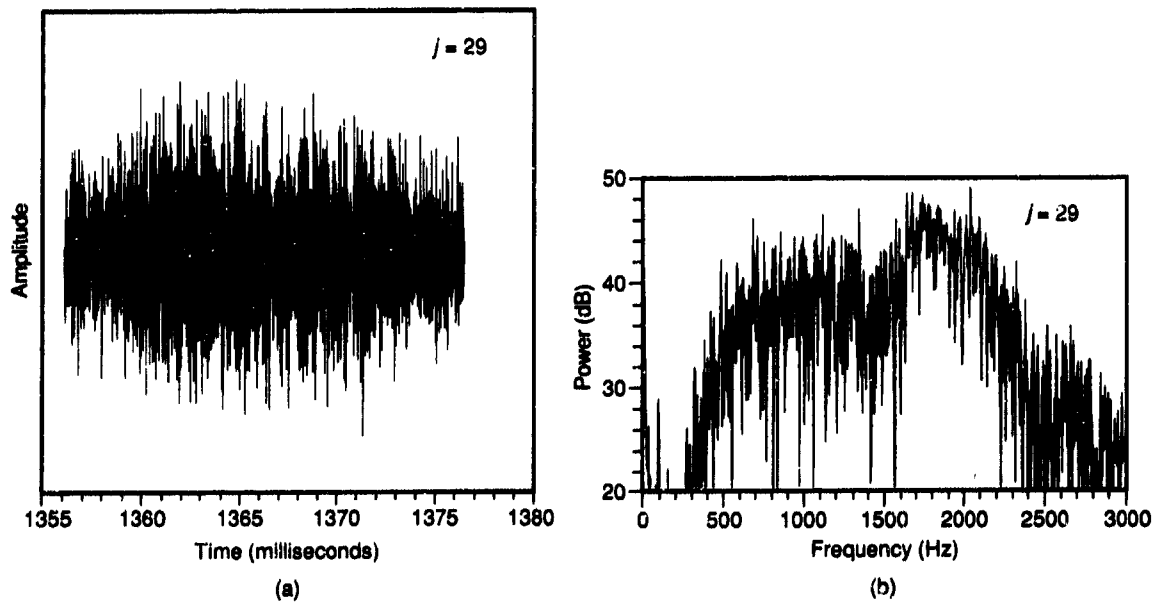


Figure 21. Received PAEL signal at $r = 1710$ -meter element.

Digital complex bandshifting of the AEL band is accomplished efficiently by the $f_s = 7500$ -Hz selection since $f_s = 4f$. The bandshifting operation provides immediate reduction of the data volume.

Rapid samplers coupled with high-speed, digital-signal-processing chips offer the alternative of sampling at much higher frequencies, followed by digital filtering and decimation. This approach has also been successfully implemented and used to process PAEL data sets.

Linear quantization is performed over the expected dynamic range of the analog audio signal. Fine quantization is not critical in the AEL band since the PAEL signal and the methods by which it is processed are quite robust. The number of bits required to quantize a sample is, therefore, determined by the beamforming band requirements.

Propagation-delay-time measurements have been repeatedly performed on the various data sets by several investigators. Success of each processing implementation is testimony to the robustness of the PAEL design.

Figure 22 presents matched-filter responses of the received signals displayed in figures 20 and 21 using the PAEL signal replica of figure 19.

The insets allow close examination of the correlations attributable to the direct-path and surface-reflected-path signal arrivals. The structure of these plots is typical of every data set in table 2.

A high degree of pulse compression is achieved by matched filtering. The peaks typically have a width of 2 ms at one-half the maximum amplitude.

Advance processing of the delay measurements prior to the geometric AEL processing was performed. This allowed at least two or three chirps to be processed for a given PAEL buoy before peaks must be classified and outliers rejected. If, for a given PAEL/receiver buoy pair, consecutive matched-filter-response plots are stacked, a three-dimensional contour, or waterfall, plot is created. The sets of direct-path peaks and surface-reflected-path peaks line up, forming what appears to be nearly parallel

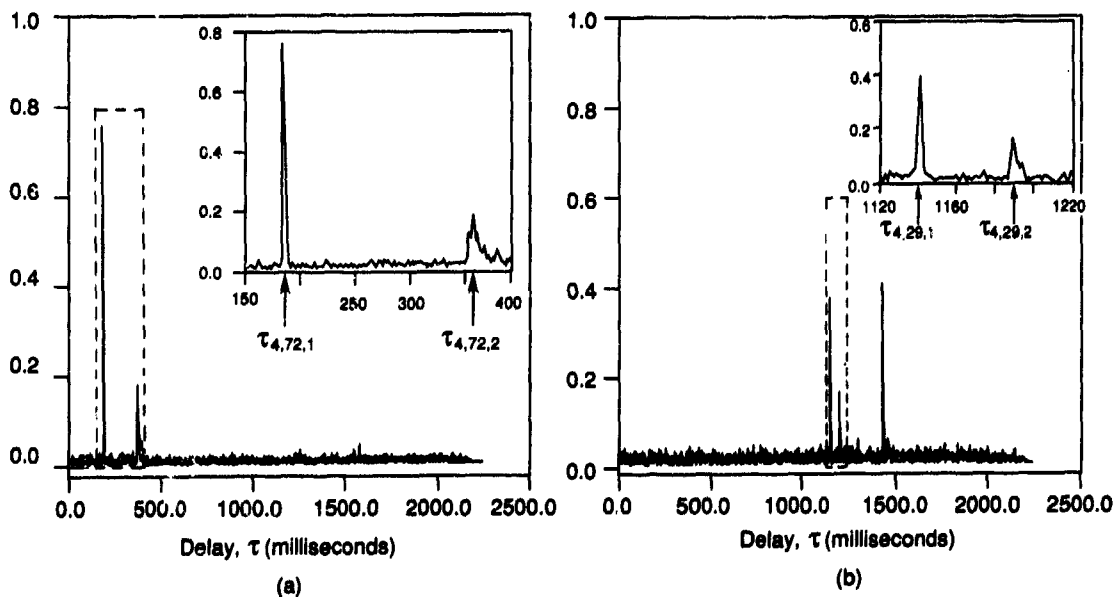


Figure 22. Matched-filter response.

chains. The randomly occurring peaks due to interfering chirps from other PAEL buoys are isolated, clearly distinguishable from the two dominant chains. The chains are spline-fitted to remove measurement errors and to create a continuous delay function.

A variation of the waterfall plot is presented in figure 23 for the two elements previously considered. Only the top 10 peaks which exceed a detection threshold are preserved. The resulting time history plots are less cluttered than those produced by standard waterfall plots. The direct-path and surface-reflected-path lines represent a time history of the multipath propagation time from the PAEL projector to these array elements.

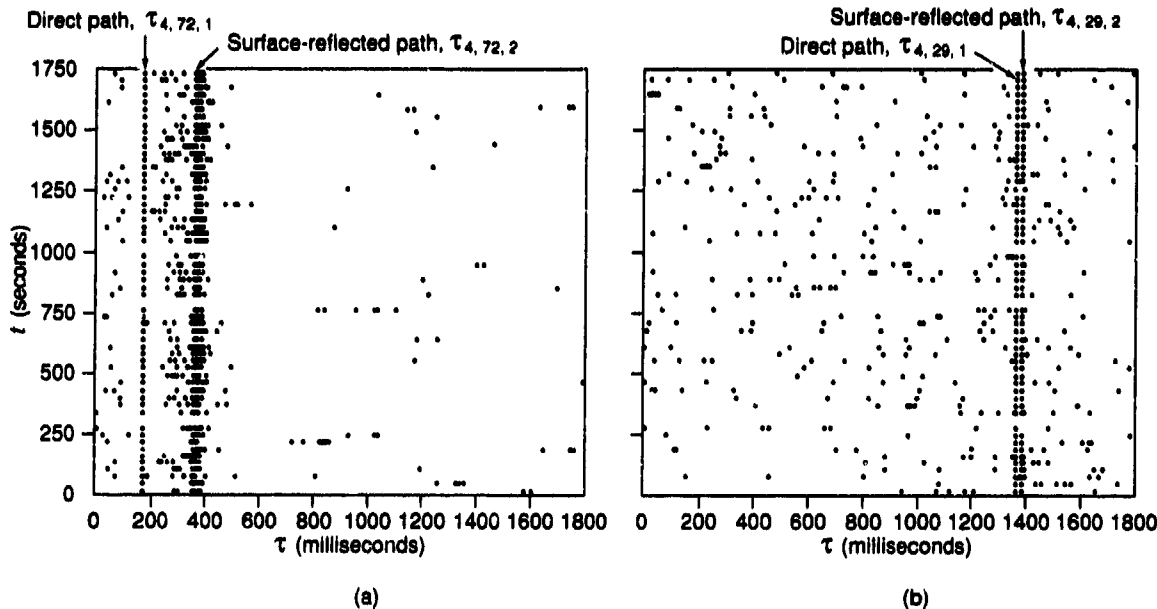


Figure 23. Time history of delay measurements.

The propagation-time measurements, τ_{ijk} , are taken from the fitted delay function and are converted to depth and range by ray tracing in the alternative manner described previously. For the present analysis, a constant gradient is fitted to the SSP predicted from the measured bathythermogram. This first-order correction of errors due to refraction has been adequate for all AEL processing performed thus far.

8.4 ARRAY ELEMENT LOCALIZATION

As a quick-look analysis of the Array 143 data set, a subarray consisting of $M = 13$ Q-53B elements has been localized using $m = 4$ PAEL sonobuoys.

A plan view of the buoy field is presented in figure 24. PAEL $i = 1$ determines the origin of the pinger-defined coordinate system. PAEL $i = 2$ fixes the x' -axis. Dashed vectors indicate the propagation paths measured by figures 22 and 23.

8.5 BEAMFORMING

Several beamforming methods for large aperture, horizontal random arrays are available (Johnson, 1982). Adaptive beamforming (ABF) techniques, where directional noise is adaptively nulled, is superior to conventional beamforming approaches (CBF) in many instances. In general, ABF offers a substantial reduction in both noise mean level and spatial background variance at the processor output. Although ABF is more sensitive to AEL errors than CBF, the inherent processing gains of ABF should outweigh the losses due to these errors.

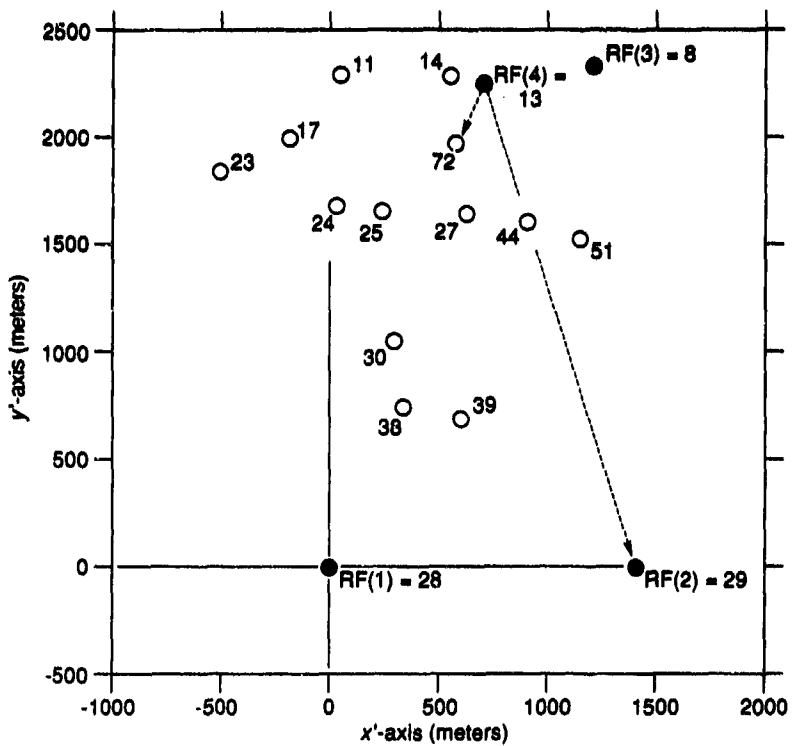


Figure 24. Plan view of subarray of Array 143.

The average input SNR of the individual omnidirectional hydrophone elements is obtained by using the average power for the frequency bin of interest, $\bar{S}/\bar{\pi}$. Assuming that the noise is broadband, input noise power, $\bar{\pi}$, is estimated by averaging the element powers for frequency bins near the bin of interest (two guard bins on either side are excluded) to obtain $\bar{\pi} \approx \bar{n}$. Then

$$\bar{S}/\bar{\pi} \approx \frac{\bar{S}+\bar{N}}{\bar{\pi}} - 1. \quad (47)$$

The beamformed array output signal-to-noise power for the bin of interest is computed similarly using the steered beamformer powers,

$$\bar{S}/\bar{N} \approx \frac{\bar{S}+\bar{N}}{\bar{N}} - 1. \quad (48)$$

Array signal gain and array noise gain are estimated with

$$G_s = \frac{\bar{S}}{\bar{S}} \approx \frac{\bar{S}+\bar{N}-\bar{N}}{\bar{S}+\bar{N}-\bar{n}}. \quad (49)$$

$$G_n = \frac{\bar{N}}{\bar{\pi}} \approx \frac{\bar{N}}{\bar{\pi}}. \quad (50)$$

Measured array gain, obtained by substituting equations (47) and (48) into equation (1), is compared to the theoretically achievable array gain, $10 \log M$.

9.0 CONCLUSION

A prototype version of an AEL sonobuoy, the PAEL sonobuoy, has been developed. Hydrophone localization in experimental sonobuoy arrays using PAEL sonobuoys has been successfully demonstrated.

Array-element localization and preliminary beamforming results have confirmed the suitability of the AEL sonobuoy design and the AEL signal parameters. No problems have been observed that would prompt any major design changes.

10.0 RECOMMENDATIONS

Based on experience with the PAEL sonobuoy, only minor design changes in the next-generation AEL sonobuoy are recommended. These include

- a. implementing a reversing FM sweep direction for successive chirps;
- b. adjusting the AEL signal envelope to take full advantage of the improved transducer response; and
- c. increasing the detectability of the start pulse.

These refinements may be carried out with the present digital PAEL design by merely altering the firm-ware. Generally tightened tolerances throughout the specification are feasible, perhaps to the extent that fixed matched filters can be used instead of individually derived matched filters based on transmitted replicas.

If DIFAR sonobuoys remain the basis of the array system, future AEL sonobuoys should be manufactured by modifying the newer Q-53D sonobuoy.

Quantitative performance measurements of the AEL system under tightly controlled conditions are still required. A stationary acoustic source projecting multiple tones at multiple source levels is suggested. By examining array gain as a function of these parameters, the utility of sonobuoy arrays for specific applications may be determined.

11.0 NOMENCLATURE

α	absorption coefficient
β	bandwidth
β_Δ	bandwidth of chirp pulse
β_{eff}	effective bandwidth
Δ	chirp-pulse frequency excursion
θ_{gr}	grazing angle of ray at sea surface
θ_{or}	orientation angle of array
θ_{st}	beam steering bearing angle
θ_{tr}	trilateration angle at array element
λ	acoustic wavelength

λ_{\max}	maximum beamforming wavelength
λ_{\min}	minimum beamforming wavelength
σ_ϕ	rms phase error
σ_r	rms range-measurement error
σ_{xy}	rms horizontal positional error
$(\sigma_{xy})_{\text{AEL}}$	AEL element rms horizontal positional error
σ_z	rms vertical positional error
τ	time displacement
τ_j	beamforming delay applied to output of element j
τ_{ijk}	propagation time from AEL element i to element j along path k
ψ_{gr}	departure angle of ray which just grazes sea surface
ψ_{st}	beam steering elevation angle from horizontal plane
c	speed of sound
c_o	speed of sound at sea surface
$\frac{\partial c}{\partial z}$	vertical sound-speed gradient
dr_{xy}	horizontal range-measurement error
dr_z	vertical range-measurement error
DI	directivity index
DI _o	error-free directivity index
f	frequency measured in Hz
f_{\max}	maximum beamforming frequency
f_{\min}	minimum beamforming frequency
f_s	sampling frequency
f_c	carrier frequency or center frequency
G	main response axis gain
G_o	error-free main response axis gain
G/G_o	fractional loss in gain
$h(t)$	impulse response of filter
H	rms sea surface wave height (trough to crest)
i	identifying index of AEL projector
j	identifying index of hydrophone, including AEL sonobuoy phone
k	acoustic wave number equal to the quantity $2\pi/\lambda$
k	propagation path index

K	chirp rate (Hz/second)
m	number of AEL projectors in the array
M	number of hydrophones in the array
π	average noise power of array element
N	average noise power of array
NL	ambient noise level
PG	processing gain
r	range in units of distance
r_{ij1}	direct-path range from AEL element i to hydrophone j
r_{ij2}	surface-reflected-path range from AEL i to hydrophone j
r_{xy}	horizontal component of r
r_z	vertical component of r
$R_{ii}(\tau)$	autocorrelation function
$R_{ij}(\tau)$	cross-correlation function
$s(t)$	replica of AEL signal for matched filter
\bar{s}	average signal power of array element
SL	source level
$(SL)_f$	source level at the center frequency
\bar{S}	average signal power of array
$(S/N)_{in}$	signal-to-noise ratio at input to signal processor
$(S/N)_{out}$	signal-to-noise ratio at output of signal processor
t	time
t_0	start time of AEL signal projection
t_{ijk}	time tag associated with s_{ijk} measurement
T_{ar}	time required for propagation across array aperture
T_{sig}	AEL signal duration
$(T_{sig})_{eff}$	effective AEL signal duration
TL	transmission loss
w	normalized weighting coefficient
$x_j(t)$	audio time series produced by array element j
$y_{ij}(t)$	matched-filter output
z	depth below sea surface

12.0 GLOSSARY

ABF	adaptive beamforming
A/D	analog-to-digital
AEL	array-element localization
CB	conventional beamforming
CEP	circular equal probability
dB	decibels
DI	directivity index
DIFAR	directional LOFAR
GDOP	geometric dilution of precision
Hz	hertz
kHz	kilohertz
km	kilometers
LOFAR	low-frequency analysis and recording
m	meters
MHz	megahertz
min	minute
ms	milliseconds
PAEL	Prototype AEL
RAYMODE	Navy sound propagation model
RF	radio frequency
rms	root mean square
s	seconds
SL	source level
SM	safety margin
SNR	signal-to-noise ratio
SSP	sound-speed profile
TL	transmission loss
VHF	very high frequency
VLF	very low frequency

13.0 REFERENCES

Aki, K. and P. G. Richards. 1980. *Quantitative Seismology, Vol. II*, W. H. Freeman and Co., San Francisco, CA.

Burdick, W. S. 1984. *Underwater Acoustic System Analysis*, Prentice-Hall, Edgewood Cliffs, NJ.

Cheung, J. Y. May 1978. "Array Element Location System," Boeing Computer Services Company Report no. AM-49.

Cheung, J. Y. and A. W. Warren. April 1978. "GDOP Analysis of the Array Element Location System," Boeing Computer Services Company Report No. AM-43.

Duckworth, G. L. November 1987. "A Robust Algorithm for Tracking of Drifting Acoustic Arrays in the Arctic," *Proc. IEEE 21st Asilomar Conference*, Pacific Grove, CA.

Eby, E. S. December 1967. "Frenet Formulation of Three-Dimensional Ray Tracing," *J. Acoust. Soc. Am.*, vol. 42, no. 6.

Gill, P. E., W. Murray, M. H. Wright. 1981. *Practical Optimization*, Academic Press, London.

Hunt, M. M., W. M. Marquet, D. A. Moller, K. R. Peal, W. K. Smith, R. C. Spindel. December 1974. "An Acoustic Navigation System," Woods Hole Oceanographic Institution Report 74-6.

Johnson, Don H. September 1982. "The Application of Spectral Estimation Methods to Bearing Estimation Problems," *Proc. IEEE*, vol. 70, no. 9.

Klauder, J. R., A C. Price, S. Darlington, and W. J. Albersheim. July 1960. "The Theory and Design of Chirp Radars," *The Bell System Technical Journal*, vol. 39, no. 4.

Knudsen, V. O., R. S. Alford, and J. W. Emling. September 1944. *Survey of Underwater Sound, Report No. 3, Ambient Noise*, 6.1-NDRC-1848.

Lo, Y. T. May 1964. "A Mathematical Theory of Antenna Arrays with Randomly Spaced Elements," *IRE Trans. Antennas Propag.*

Lo, Y. T. September 1965. "Sidelobe Level of Nonuniformly Spaced Antenna Arrays," *IEEE Trans. Antennas Propag.*

Lowenstein, C. D. and J. D. Mudie. 1967. "On the Optimization of Transponder Spacing for Range-Range Navigation," *J. Ocean Technology*, vol. 1, no. 2.

Mackenzie, K. V. September 1981. "Nine-Term Equation for Sound Speed in the Oceans," *J. Acoust. Soc. Am.*, vol. 70, no. 3.

Officer, C. B. 1958. *Introduction to the Theory of Sound Transmission*, McGraw-Hill, New York, NY.

Rice, J. A. 1990. *Hydrophone Localization in a Random Sonobuoy Array*, University of California, San Diego, CA.

Ross, D. 1987. *Mechanics of Underwater Noise*, Peninsula Publishing, Los Altos, CA.

Steinberg, B. D. 1976. *Principles of Aperture and Array Systems Design*, John Wiley & Sons, New York, NY.

Thorp, W. H. October 1965. "Deep Ocean Sound Attenuation in the Sub- and Low-Kilocycle-per-Second Region," *J. Acoust. Soc. Am.*, vol. 38, no. 4.

Urick, R. J. 1983. *Principles of Underwater Sound for Engineers*, McGraw-Hill, New York, NY.

Wehner, D. R. 1987. *High Resolution Radar*, Artech House, Norwood, MA.

Wenz, G. M. December 1964. "Acoustic Ambient Noise in the Ocean: Spectra and Sources," *J. Acoust. Soc. Am.*, vol. 34, no. 12.

REPORT DOCUMENTATION PAGE

Form Approved
OMB No. 0704-0188

Public reporting burden for this collection of information is estimated to average 1 hour per response, including the time for reviewing instructions, searching existing data sources, gathering and maintaining the data needed, and completing and reviewing the collection of information. Send comments regarding this burden estimate or any other aspect of this collection of information, including suggestions for reducing this burden, to Washington Headquarters Services, Directorate for Information Operations and Reports, 1215 Jefferson Davis Highway, Suite 1204, Arlington, VA 22202-4302, and to the Office of Management and Budget, Paperwork Reduction Project (0704-0188), Washington, DC 20503.

1. AGENCY USE ONLY (Leave blank)		2. REPORT DATE December 1990		3. REPORT TYPE AND DATES COVERED Final: June 1986 – August 1990	
4. TITLE AND SUBTITLE A PROTOTYPE ARRAY-ELEMENT LOCALIZATION SONOBUOY				6. FUNDING NUMBERS PE: 64261N PROJ: 54ST7001 ACC: DN288651	
6. AUTHOR(S) J. A. Rice					
7. PERFORMING ORGANIZATION NAME(S) AND ADDRESS(ES) Naval Ocean Systems Center San Diego, CA 92152-5000				8. PERFORMING ORGANIZATION REPORT NUMBER NOSC TR 1365	
9. SPONSORING/MONITORING AGENCY NAME(S) AND ADDRESS(ES) Chief of Naval Research 800 N. Quincy Street Arlington, VA 22217-5000		Naval Air Systems Command Washington, D.C. 20381-0001			
11. SUPPLEMENTARY NOTES					
12a. DISTRIBUTION/AVAILABILITY STATEMENT Approved for public release; distribution is unlimited.			12b. DISTRIBUTION CODE		
13. ABSTRACT (Maximum 200 words) <p>Sonobuoys are used individually to sense underwater acoustic signals. A coherently processed, beamformed array of sonobuoys could result in a powerful, highly directional, large-aperture sensor. For the sonobuoy array concept to succeed, the relative locations of the individual array hydrophones must be determined and tracked.</p> <p>This report presents a design of an array-element localization (AEL) sonobuoy after considering sonobuoy array properties, environmental influences, candidate sonobuoy array elements, and AEL accuracy. This AEL sonobuoy design is validated using experimental results from a prototype implementation.</p>					
14. SUBJECT TERMS random array sonobuoy array array gain underwater acoustics beamforming plane-wave signals array-element localization acoustic ranging sonar hydrophones sound-speed profiles				15. NUMBER OF PAGES 62	
				16. PRICE CODE	
17. SECURITY CLASSIFICATION OF REPORT UNCLASSIFIED		18. SECURITY CLASSIFICATION OF THIS PAGE UNCLASSIFIED		19. SECURITY CLASSIFICATION OF ABSTRACT UNCLASSIFIED	
				20. LIMITATION OF ABSTRACT SAME AS REPORT	

INITIAL DISTRIBUTION

CODE 0012	Patent Counsel	(1)
CODE 0144	R. November	(1)
CODE 50	J. D. Hightower	(1)
CODE 54	J. Richter	(1)
CODE 541	M. Morrison	(1)
CODE 541	V. McDonald	(1)
CODE 541	R. Shockley	(1)
CODE 541	J. Rice	(20)
CODE 605	Lt. K. Garber	(1)
CODE 605	B. Shaw	(1)
CODE 605	S. Sullivan	(1)
CODE 632	D. Davison	(1)
CODE 635	J. Alsup	(1)
CODE 651	M. Nicholson	(1)
CODE 651	J. Straus	(1)
CODE 652	L. Shook	(1)
CODE 702	R. Hearn	(1)
CODE 705	N. Booth	(1)
CODE 712	P. Hanson	(1)
CODE 761	G. Byram	(1)
CODE 921	J. Puleo	(1)
CODE 934	E. Schaefer	(1)
CODE 961	Archive/Stock	(6)
CODE 964	Library	(3)

Defense Technical Information Center
Alexandria, VA 22304-6145 (4)

NOSC Liaison Office
Washington, DC 20363-5100 (1)

Center for Naval Analyses
Alexandria, VA 22302-0268 (1)

Naval Air Development Center
Warminster, PA 18974-5000 (2)

Naval Avionics Center
Indianapolis, IN 46219 (1)

Naval Air Systems Command
Washington, DC 20361-0001 (2)

Patrol Wings Ten
Moffett Field, CA 94035-5022 (1)

Patrol Wings Five
Brunswick, ME 04011 (1)

University of California, San Diego
Scripps Institution of Oceanography
La Jolla, CA 92093-0701 (3)

Pennsylvania State University
Applied Research Laboratory
State College, PA 16801 (1)

University of Texas at Austin
Applied Research Laboratory
Austin, TX 78713-8029 (1)

University of Washington
Applied Physics Laboratory
Seattle, WA 98105 (1)

BBN Systems & Technologies Corp.
Cambridge, MA 02238 (1)

Lockheed Aeronautical Systems Co.
Burbank, CA 91520 (1)

Magnavox
Garrett, IN 46738 (1)